

Author responses to:

Interactive comment on “Modeling anaerobic soil organic carbon decomposition in Arctic polygon tundra: insights into soil geochemical influences on carbon mineralization” by Jianqiu Zheng et al.

We appreciate comments from both reviewers and the editor, and have used these to extensively revise our manuscript. This document includes responses to the Associate Editor's comments and reproduces our responses to both reviewers' comments that were previously uploaded. Finally, this document includes a comparison of the revised 10 manuscript with the originally submitted version. These changes were extensive and substantially improved the manuscript's readability. Note that figures were renumbered in the revised version.

Editorial comments

15 *Both reviewers appreciate the modelling efforts conducted and indicate its importance. At the same time though, both indicate to have had major problems with the flow of the story line and with the lack of details on some crucial points of the modelling. Both need to be significantly improved to become acceptable.*

My suggestion would be to:

20 *- eliminate the extensive descriptions of the sites and the performed incubation experiments. These experiments certainly do not constitute the novel part of this manuscript (numerous similar results from similar experiments are available in literature) and it is now distracting (e.g. why extensively discussing Q10 while - I hope- it would be an emergent property from a mechanistic model?). essentials can be moved to suppl. info.*

25 We moved essential elements of the data synthesis to supplemental text. Our re-analysis of these incubation experiment results required a significant effort, and we hope the product will be useful to future investigators through the dataset that will be available as a DOI.

30 *- start the methods with a proper model description, possibly using and extended version of fig 2 to guide the flow, then model validation and then model sensitivity. The results section can start with what is now 3.3.*

35 The revised manuscript includes an extensive description of the model, with the model-data integration illustrated in a new process diagram in Supplementary Figure S2.

I also have a number of additional comments:

40 *35 - To me, model validation while using a number of initial state var. is quite fine (and is less confusing to me than model initiation), but I don't understand why measured pH was used as parameter in that analysis after the extensive discussion of the authors in the introduction that pH estimates should be based on mechanisms. If you use pH to initialize the model, it does not seem based on mechanisms. Or, to put it more generally: how mechanistic is your model and what is your scientific advance on this topic.? That does nowhere become clear and is also related to my next two comments:*

45 While geochemical speciation calculations could theoretically estimate pH based on complete measurements of dissolved charged species, this is not practical (or accurate) for Arctic soil water. In our experience, charge balance is usually very poor in these calculations due to the significant contribution of anionic dissolved organic matter, creating large errors in initial pH estimates. This illustrates the importance of the aqueous phase model that we introduce in this work. We recommend usually readily available pH measurements to initialize this model, and our mechanistic pH response function to simulate pH changes from that initial parameter over time.

50 *50 - I (and one of the reviewers too) have problems with some claims on the lack of anaerobic decomposition in ESMs. The authors are well aware, I believe, of the ensemble of ESMs developed to model global methane emissions, each of which take anaerobic decomposition processes into account (incl. a model from the CLM family if I am not mistaken). So, how should we see the advance made by this model in this respect?*

55 The revised manuscript better distinguishes the present explicit representation of anaerobic carbon decomposition cascades and redox processes from previous models that treat processes implicitly. We refer readers to our previous review in this journal by Xu et al. 2016, which provides a more comprehensive description of methane cycle models and a detailed comparison of model structures.

- The authors next argue that mechanisms should be included and indicate that Eh and pH of models should be

based on (thermodynamic) mechanisms. Such models are available and extensively used (e.g. in modelling the dynamics in anaerobic sludge reactors, but also for anoxic soil systems) and some of those models are explicitly based on humic acids and/or iron reduction. Moreover, from the current description it does not seem that pH or Eh are prognostic variables in the presented model either. So again: how does the model advance our

5 understanding compared to existing models?

We substantially revised the Introduction and Methods sections to provide more details about this new model. We agree that foundational thermodynamic modeling of anaerobic digestors and batch reactors has benefitted our work, for example by informing the thermodynamic models of Istok, Roden, Bethke et al. cited here. However, most of these 10 models were developed to simulate specific redox processes including relatively defined carbon substrates. We are not aware of other models that have attempted to couple a thermodynamically based microbial growth model, a substrate pool-based model, and a humic ion-binding model, to create a generic, process-rich carbon decomposition model for anoxic soils that allows simultaneous thermodynamic and pH calculations. Highly parameterized models often perform poorly when used to simulate a wide range of environmental conditions, so the present model is 15 remarkable for its fidelity in simulating CO₂ and CH₄ production from gradient of soil moisture and SOM conditions.

Referee #1

20 *The manuscript proposes a new model to study organic matter decomposition under anaerobic conditions from arctic soil with a focus on implementing the effects of temperature and pH. The research direction is of a great importance and the authors attempt to formulate such effects on carbon decomposition from arctic is also interesting. However I believe the representation of the manuscript could be significantly improved. My major concern is that the current form of presenting the manuscript is not self-standing and a lot of refers has been done to authors previous publications that makes it difficult to follow and evaluate the content efficiently.*

25 One of the main goals in this paper (anaerobic model development) is to develop mechanistic representation of methanogenesis, iron reduction and associated pH feedbacks. This goal required data on soil geochemical properties, Fe(III) and Fe(II) concentrations and pH changes during incubations to be synthesized from previous publications. It is not feasible or appropriate to reproduce the high level of detail in those coordinated soil 30 geochemistry measurements, which are described in the cited material. We have moved the synthesis discussion to Supplemental Materials.

35 *Similarly, model description is not complete and no clear hierarchy of the model development and formulation is provided. I understand that the main model has been developed previously but this should not lead to a discontinuous representation that will be non-informative for audience with different background. I strongly suggest improving the model representation and at minimum including a clear schematic with explicit steps that should be taken in formulating such model.*

40 This is a good suggestion regarding better model documentation and archiving. To clarify the workflow in the manuscript, we are reorganizing the section that introduces the model and adding a new flow chart in the Supplementary Figure 2 explaining how the synthesized data product is used to inform model development. We are also including a detailed model description in the Supplementary material, supplementing Figure 2 that demonstrates the main structure of the new model. Detailed descriptions of the carbon pool cascade adopted from CLM-CN model, 45 thermodynamically-based growth equations for methanogenesis and iron reduction, and the WHAM model implementation to represent pH buffering will be included in the Supplementary material. Detailed instructions to run the model with our database (redox.dat) under PHREEQC framework will also be included with an example input file. A permanent DOI is reserved for code and additional details on model implementation.

50 *Other comments:*
- *Introduction was well-written and provided important and necessary information. However I would still encourage authors to try shortening it that would be focused on the main message of the paper.*

55 We condensed the introduction section to be more focused on introducing explicit processes that are missing from current Earth System Models (ESMs).

- While authors acknowledge the key role of hydrolysis to convert SOM (particulate organic matter) to DOC, they have simply ignored this step and no discussion is provided on how the step 1 (Figure 2, conversion of SOM to DOC) is modelled and if hydrolysis is taken into account in the current model.

Hydrolysis is generally recognized as the rate-limiting step during anaerobic carbon decomposition. As stated in the second paragraph in section 2.3, hydrolysis and fermentation include multiple reaction steps, and we combined hydrolysis and fermentation together in one step using an empirical approach. This is a practical assumption for three reasons: (1) Microorganisms that degrade cellulose anaerobically usually also ferment sugars following hydrolysis; 5 (2) Current characterization of SOM in Arctic soils is insufficient to differentiate multiple hydrolysis and fermentation steps: the few reports on Arctic soil exoenzyme activities do not survey the full range of hydrolytic reactions required for biomass decomposition such as endoglycosidases. Thus, data are not available to support multiple hydrolysis and fermentation steps in the model; (3) The lumped hydrolysis and fermentation step still allows us to use this 10 reaction as the rate-limiting step in the model, which fits the observations presented in Figure 3. We will clarify this representation of hydrolysis in the revised manuscript's introduction.

Step 1 (Figure 2, conversion of SOM to DOC) is calculated using the indirect fraction of the original respiration factor from CLM-CN carbon decomposition cascade. The detailed description is included in the commented code file (can be accessed at <https://dx.doi.org/10.5440/1430703>, once the manuscript revision is finalized). We are also including 15 detailed description in the Supplementary material.

- *How the model deals with large discharge rate of DOC that is common in permafrost soil due to lateral flow?*

20 The Barrow Environmental Observatory is located on the flat Arctic coastal plain, where lateral flow is minimal after snowmelt. Precipitation roughly balances evapotranspiration in most areas during the thaw season. Dealing with lateral flow requires transport processes, which are beyond the scope of current manuscript. However, it is a good target for future research to model different sites, and we are actively working towards coupling PHREEQC 25 capabilities (chemical equilibrium and kinetics) with thermal hydrology models to address transport.

25 - *More explanation on how fermentation step is formulated in the model would be helpful.*
- *More explanation on how parameterization has been done and how it has been used in the current model would be nice.*

30 Additional model details have been added to the Methods section. The fermentation step is parameterized as a single reaction following first order kinetics.



35 As stated in the second paragraph in section 2.3 and first paragraph in section 2.4, the above stoichiometry of fermentation reaction is a lumped process representing production of low molecular weight organic acids (in this case, acetate), CO₂ and H₂ from labile carbon (we used a constant molecular formula C₆H₁₂O₆, representing monosaccharides).

40 Methanogenesis and iron reduction are parameterized using individual growth equations of acetoclastic methanogens, hydrogenotrophic methanogens and iron reducers utilizing acetate or H₂. In the revised manuscript, we will include more detailed description on growth equations, and a summary of kinetic rate constants and half saturation constants in the Supplementary material.

45 - *Q10 values are represented as soil layer combinations. Was there no effect of soil layer? Or there is a correlation with soil depth? More explanation would be helpful.*

50 The initial production rates of CO₂ and CH₄ used for Q10 calculations showed strong depth effects, as demonstrated in Table S5. Thus we reported the temperature effect (Q10) using grouped soil layers. We further conducted a t-test on the estimated Q10 values for CO₂ and CH₄ production, respectively (Table S6). These analyses were mentioned in section 3.2. We will add an additional line for clarification in this section.

55 - *In schematic Figure 2, it is shown that conversion of SOM to DOC produces CO₂? What is the process for this production? Is it general?*

60 In the original CLM-CN carbon decomposition cascade, each carbon pool is associated with a respiration factor representing carbon loss as CO₂. Now in our new model, this factor is split into a direct fraction that is respiration to CO₂, and an indirect fraction that goes to DOC pool. We kept the direct fraction to represent microbial respiration.

CO₂ production is also required in anaerobic systems for microbial biomass formation: forming reduced cellular components such as lipids must be offset by CO₂ production to balance electrons in the system. In the revised manuscript we will address this briefly in the discussion of Figure 2 and add more detailed explanations in the Supplementary material.

5

- *Representation of Table 1 should be improved. Is table 1 and Table S4 representing different system? Please be clear in the captions of the Tables.*

10 Gas production data used in the statistical analysis in Table 1 are converted to per gram carbon basis, while in Table S4, data are reported on per gram dry soil basis. The reason we decided to report two tables is due to the high correlations of WEOC, TOAC and soil moisture in respect to SOC. Such correlations conceal the relationships between gas production and other soil geochemical properties. Though it was briefly mentioned in the first paragraph of section 3.2, we will clarify the differences in the revised manuscript and highlight the differences between two

15 tables.

- *In the text, it is mentioned that "The maximal production of CO₂ is about 2/3 of the initial carbon." Where this number came from?*

20 This calculation is based on the stoichiometries of equation A1, A2 and A4. When starting with 1 mol of labile carbon (C₆H₁₂O₆), 1/3 of the carbon is released as CO₂ during fermentation, and 2/3 of the carbon forms acetate, which can be further respiration as CO₂ via methanogenesis (1/3 of initial carbon) or iron reduction (2/3 of initial carbon). We will replace this sentence with a more general statement: For complete mineralization, the fraction of initial carbon

25 respired as CO₂ is in the range of 2/3-1.

- *What "process rich carbon decomposition model" mean?*

30 That statement means that we explicitly included mechanistic representations of chemical equilibrium processes to allow simultaneous thermodynamic and pH calculations. We will clarify this in the revised manuscript.

- *In Figure 8, could you also show the data at 8C which other data points are normalized with? Is only two data points enough to make a conclusion? How do you illustrate huge variations in observation data? What are the actual values for CO₂ and CH₄ production rates at 8C? Is it for observations? Is absolute data are comparable? Where is the Shaded area mentioned in the caption?*

40 Data at -2 and 4 °C in this figure are normalized to rates measured at 8 °C from corresponding soil samples. i.e. the value for each point at 8 °C is set to 1 in respect to the y-axis scale in the figure. There were 14 averaged observed values for each temperature (each representing a unique soil microtopographic feature × soil layer combination). The absolute values of CO₂ and CH₄ production rates are plotted in Figure 4 for each temperature. There are huge variations in observations among different soil microtopographic feature × soil layer combinations. We will clarify this interpretation in the revised manuscript.

45 The shaded areas are plotted around each colored line representing model simulations using different temperature response functions. They are quite small, indicating stronger model uncertainties generated from different functions rather than the designated time scale used to run model simulations.

50 - *In Figure 3, notations for Figure 3a are not clear. For example LCP-C1-0?*

The notations of treatment (soil microtopographic feature × soil layer combination) are summarized in Table S1. For example, LCP-C1-O means Low Centered Polygon-Center (the first soil core)- Organic layer. LCP-C2-M means Low Centered Polygon-Center (the second soil core)- Mineral layer. With these notations one can easily identify the microtopographic feature from the figure. We will add an additional line referencing Table S1 for clarity in the revised manuscript.

- *In general, I found it difficult to follow the model results in the form that are represented in Figures 3, 6 and 7, 9. Is there a simpler way of showing the model results that one could extract the trends?*

Figure 3 is a bar graph showing changes in WEOC and TOAC pool after incubation. Factors we here include different soil microtopographic feature \times soil layer combinations, three different incubation temperatures, and variations among triplicate incubations. All these are essential to demonstrate why we made the model assumption
5 that the DOC pool is in equilibrium state, and the rate-limiting step is the fermentation of DOC into organic acids (Figure 2, process 2).

Figure 6, 7 and 9 are model sensitivity analyses. Variations of $\pm 25\%$ and $\pm 50\%$ were applied to tested parameters (x-axis), the resulting output changes were plotted in bars (y-axis). For example, in Figure 6, when the initial pH is
10 decrease by 8% and 17%, CH₄ production decreased by 40% and 80%, respectively. We will provide such an example in the revised text to clarify interpretation.

15

Referee#2

*This paper examines aerobic and anaerobic soil organic matter decomposition in the context of iron, and pH. This is an important contribution to the understanding of soil carbon dynamics in permafrost regions which hold vast
20 reservoirs of carbon that could potentially be released under future climate change. Unfortunately, this manuscript has flow problems with substantial logical gaps between a traditional correlative analysis and the process rich model. More concerning is a lack of documentation on how the process rich model was developed, making the simulation results of this study unreproducible as is. This paper tries to do both a traditional regression/correlation style analysis and a nonlinear process rich simulation. From what I can tell the traditional analysis is solid, although the lack
25 analysis scripts make it difficult to evaluate. However, the connection to the process rich simulation is tenuous at best. In addition, I'm not clear how the data was incorporated into the simulation and how the simulations were validated with the data. I would consider splitting this into two papers, one with the traditional analysis and a second with the model development, parameterization, and validation. While this is not required it would make the manuscripts easier to write. As is there remains work needed on the flow and connection between these two
30 components.*

We appreciate the positive feedback on the synthesis data analysis and the constructive suggestions on making the connections between data synthesis and model development. We moved the data synthesis discussion to the Suplemental materials. To clarify the workflow in the manuscript, we are revising the model introduction (section 2.3) 35 and adding a new flow chart explaining how the synthesized data product is used to inform model development. For example, the bar graph showing changes in WEOC and TOAC pool after incubation (Figure 3) is the motivation to make the model assumption that DOC pool is in equilibrium state, and the rate-limiting step is the fermentation of DOC into organic acids (Figure 2, process 2).

40 We are also including a detailed model description in the Supplementary material. While Figure 2 demonstrated the main structure of the new model, a revised version of Figure 2 will include the complete CLM-CN carbon decomposition cascade (including the litter pools that currently we are not using in our model) to demonstrate how the carbon pools are adopted from CLM-CN model and modified for our modeling purpose. The new modeling components developed in this work, including thermodynamically-based parameterization for methanogenesis and 45 iron reduction, and WHAM model implementation to represent soil pH buffering, are discussed in great detail in the Supplementary material.

I would like to see some discussion of scaling of these microscale processes to macroscale models.

50 We expanded our current discussion in section 4.4.

This study needs a lot more detail to make model development reproducible. The link to github code is a start but documentation is completely inadequate and lack of permanent DOI on the repository means that the codebase might not be there for future studies. The code needs to be commented with major algorithms summarized in 55 functions. README needs instructions on running codebase with a summary of the content of each file. Alternatively this could be submitted as a markdown file with input-function-output format with inline comments explaining approach. Include version number for PHREEQC. Right now, I would not consider this study to be reproducible and it is difficult to evaluate the model results without this context.

We appreciate these suggestions to improve model documentation. Currently the commented model is in the writephrq.py file. To make the model easier to follow, we have added step-by-step instructions on the github site, including PHREEQC installation, how to run the model with our database (redox.dat), and how to create PHREEQC executable .phrq files using the python script we have provided. A permanent DOI is reserved for model code and 5 additional details on model implementation is included. We will include example input and output files with detailed comments. It will be publicly accessible once we finalize the manuscript.

10 *I'm concerned that the authors both use a simple correlation analysis to argue for inclusion of various dependent variables in the proposed highly complex non-linear model. In particular, I would not have expected a strong correlation between moisture and SOC given the typical non-linear sensitivity function used to describe respiration response to moisture (though this is possibly explained by the range of moisture conditions considered). In addition, low correlations could be explained by non-linear responses. At the risk of adding yet another analysis to an already confusing study, I would suggest that instead the authors use a paired scatter plot to visually show the relationships 15 between these variables. This will demonstrate that there is no strong non-linear relationship and that the correlation coefficients are sufficient to describe the relationship.*

20 The correlation between soil moisture and SOC is indeed an interesting result. Measurements of total soil carbon are highly correlated with gravimetric water content in BEO soils (Pearson $r = 0.80$, $P < 0.0001$). We will include a paired scatter plot in the revised version. We suggest several alternative explanations. First, high water content in saturated areas preserves organic matter by limiting oxygen diffusion, as the reviewer notes below. Second, undecomposed organic matter binds water tightly, even at low matric potential. Third, high organic matter composition creates large 25 pore volumes that fill with water in saturated soils.

25 *Line by line reactions:*
P1L23 *While anaerobic decomposition certainly is missing from many ESMs, I'm not sure I would claim that it is the main driver for model uncertainty. There are several processes which could improve model performance that are 30 currently being investigated and this tripped me up reading through the abstract.*

We agree that the statement is oversimplified. We will change that to "one of the reasons" driving model uncertainty in saturated soils.

35 *P3L5 Models traditionally do however consider O₂ limitation with increasing moisture saturation. I'm almost certain that the authors are aware that traditional moisture sensitivity functions are typically rationalized to have decreasing decomposition under high moisture due to limited O₂ diffusion (Orchard and Cook 1983). What this typically does not extend to CH₄ emissions, it does implicitly include anaerobic decomposition. A review of implicit vs explicit process representation in decomposition models may be more appropriate here than an outright claim that anaerobic 40 decomposition is not included in ESMs.*

45 Yes, we are aware of the use of moisture functions as a proxy of decomposition level. The suggested term of "implicit vs explicit" is a very nice summary of the problem we were trying to identify in current ESMs. We will summarize implicit vs explicit approaches used in current ESMs to simulate carbon decomposition under anaerobic conditions.

P4L28 *60days is a short incubation to try to fit a full soils model to. I want to see concerns about time scale addressed somehow here.*

50 The length of incubation time was selected because the thaw season in Barrow is about 60-90 days. We have briefly mentioned this in the model development section, as the short incubation is the main reason we adopted the CLM-CN carbon decomposition cascade, since we have no data to fit a full carbon model. We will add additional discussions in both section 4.3 and 4.4 to talk about the limitations of model validation from current datasets and some future considerations.

55 P4L38 *Why was the 4C dropped from the Q10 calculation??*

Originally, we fitted the data from 3 different incubation temperatures. There was no significant difference between the Q10 values estimated by two approaches. We added an additional line to clarify.

P5L2 *These package citations are less useful without the associated analysis script. Could this please be included in either the SI or as a separate DOI citation?*

We believe the statistical analysis packages listed here are well documented and applied in this project using
5 standard methods. We will clarify this sentence and provide scripts that are essential for model development through
online distribution (see below).

P5L12 *Please be go into more detail on the adaptation of CLM here. Figure 2 is extremely useful but this could use more detail here or in the SI. I would urge the authors to restate the model formulation (even when explicitly drawing
10 on previous work) since frequently it is not clear what portions were modified for the current model. Please include a set of full mathematical equations, descriptions appropriate algorithms, and a fully commented code base used to run the models.*

In the revised manuscript, all these will be included in the Supplementary material. A DOI citation will be available for
15 both model code and synthesized data product (can be accessed at <https://dx.doi.org/10.5440/1430703>, once the manuscript is finalized). A fully commented code base and step-by-step instruction will be provided with example
input and output files. Readers will be able to run our scripts from their own computers.

P6L5 *Well that is certainly creative model initialization.*

20 Thank you!

P6L22 *'further adjusted' Could the authors clarify? Right now it reads as an 'expert tuned' model which is not current best practices given the range of parameter fitting tools that exist.*

25 This is a good suggestion. We do not have valid data to verify the biomass of specific functional groups. This lack of data is due to the technical challenges we are facing while doing DNA and qPCR based quantifications. That's the main reason we used thermodynamically-based growth equations to build microbial biomass directly into reaction kinetics. However, we still need a starting point of gross microbial biomass estimations, so the values were selected
30 from previous modeling work done in the Arctic regions. We will add additional explanations in the revised manuscript.

P6L25 *This feels like a very limited sensitivity analysis. An a priori 50% uncertainty seems to be a relatively tight bound for a soil model, especially given the 3 orders of magnitude that was mentioned previously.*

The main purpose of sensitivity analysis is to demonstrate the direction and magnitude of changes. We agree that additional sensitivity analysis on these parameters would be helpful. In the revised manuscript, we added additional sensitivity analysis in Figure 7.

40

P8L7 *How was the model calibrated?*

The model was calibrated by fitting both CO₂ and CH₄ production data in two separate steps. We are adding a flow
45 chart explaining how the synthesized data were incorporated into model development and validation.

P9L18 *Was this perturbation analysis done independently of the previous perturbations?*

Yes, the perturbation analysis was done independently of previous perturbations.

50

Modeling anaerobic soil organic carbon decomposition in Arctic polygon tundra: insights into soil geochemical influences on carbon mineralization

Formatted: Font: 16 pt

5 Jianqiu Zheng¹, Peter E. Thornton^{2,3}, Scott L. Painter^{2,3}, Baohua Gu², Stan D. Wullschleger^{2,3}, David E. Graham^{1,3}

Deleted:

¹Biosciences Division, Oak Ridge National Laboratory, Oak Ridge TN, 37931 USA

²Environmental Sciences Division, Oak Ridge National Laboratory, Oak Ridge TN, 37931 USA

³Climate Change Science Institute, Oak Ridge National Laboratory, Oak Ridge TN, 37931 USA

10

Correspondence to: David E. Graham (grahamde@ornl.gov)

This manuscript has been authored by UT-Battelle, LLC, under contract DE-AC05-00OR22725 with the US Department of Energy (DOE). The US government retains and the publisher, by accepting the article for publication, acknowledges that the US government retains a nonexclusive, paid-up, irrevocable, worldwide license to publish or reproduce the published form of this 15 manuscript, or allow others to do so, for US government purposes. DOE will provide public access to these results of federally sponsored research in accordance with the DOE Public Access Plan (<http://energy.gov/downloads/doe-public-access-plan>).

Abstract. Rapid warming of Arctic ecosystems exposes soil organic matter (SOM) to accelerated microbial decomposition, 20 potentially leading to increased emissions of carbon dioxide (CO₂) and methane (CH₄) that have a positive feedback on global warming. Current estimates of the magnitude and form of carbon emissions from Earth system models include significant uncertainties, partially due to the oversimplified representation of geochemical constraints on microbial decomposition. Here we 25 coupled modeling principles developed in different disciplines, including a thermodynamically based microbial growth model for methanogenesis and iron reduction, a pool-based model to represent upstream carbon transformations, and a humic ion-binding model for dynamic pH simulation to build a more versatile carbon decomposition model framework that can be applied to soils under varying redox conditions. This new model framework was parameterized and validated using synthesized anaerobic 30 incubation data from permafrost affected soils along a gradient of fine-scale thermal and hydrological variabilities across Arctic polygonal tundra. The model accurately simulated anaerobic CO₂ production and its temperature sensitivity using data on labile carbon pools and fermentation rates as model constraints. CH₄ production is strongly influenced by water content, pH, methanogen 35 biomass, and presence of competing electron acceptors, resulting in high variability in its temperature sensitivity. This work provides new insights into the interactions of SOM pools, temperature increase, soil geochemical feedbacks, and resulting CO₂ and CH₄ production. The proposed anaerobic carbon decomposition framework builds a mechanistic link between soil geochemistry and carbon mineralization, making it applicable over a wide range of soils under different environmental settings.

Deleted: The fate of permafrost carbon is determined in large part by soil moisture, and a significant portion of carbon may thaw in wet, anoxic conditions.

Deleted: since

Deleted: models do not explicitly represent anaerobic carbon

Formatted: Font: (Default) Cambria, Font color: Black, Pattern: Clear

Deleted: fermentations

Deleted: 1

Deleted: presented here

Deleted: 1

35 1 Introduction

The northern permafrost region contains 1400-1800 Pg soil carbon (C), which is more than twice as much C as is currently contained in the atmosphere (Tarnocai et al., 2009; McGuire et al., 2012). Persistent cold and saturated soil conditions have limited

C decomposition in this reservoir. However, rapid warming and permafrost thaw exposes previously frozen organic carbon to accelerated microbial decomposition, potentially leading to emissions of carbon dioxide (CO_2) and methane (CH_4) that have a positive feedback on global warming (Zimov et al., 2006; Schuur et al., 2015; Schuur et al., 2009). How quickly frozen soil organic matter (SOM) will be mineralized, and how much permafrost C will be released to the atmosphere following thaw is highly 5 uncertain. Earth system models project 27 -508 Pg carbon release from the permafrost zone by 2100 under current climate forcing (Zhuang et al., 2006; Koven et al., 2015; MacDougall et al., 2012; Schaefer et al., 2014), varying by a factor of thirty. Understanding environmental dependencies of soil organic matter (SOM) decomposition is therefore essential for reducing model uncertainties and improving predictions of future climate change.

10 Disagreement in model projections for the northern permafrost region could be due to differences in model structure, model initialization, or parameters used in simulations. Despite increasingly detailed process representations in many models that simulate terrestrial CO_2 and CH_4 fluxes, important geochemical and metabolic constraints might still be poorly represented, oversimplified or missing in current biogeochemical models (Xu et al., 2016). The northern permafrost region is rapidly changing in response to the changing climate. Rising temperatures not only release more labile carbon from permafrost for decomposition, but also create
15 thermal and hydrological heterogeneity that further affects biogeochemical processes. Here we examine two mechanisms that substantially affect SOM turnover in permafrost-affected soils. First, rising temperature alters the kinetics of biogeochemical reactions (Segers, 1998). This effect is more pronounced at subzero temperature (Bore et al., 2017), and the process rate increase is higher at lower temperature ranges (Davidson and Janssens, 2006). Microbial communities also change with temperature, compounding effects on process rates (Karhu et al., 2014). Models address this temperature effect using empirical functions and
20 parameters (Schädel et al., 2016), which might be highly biased depending on model assumptions, and original curve fitting techniques, generating large uncertainties. Second, heterogeneity in permafrost thaw and related hydrological responses creates geochemical gradients in soils. Models use different levels of detail to simulate effects of water saturation (Meng et al., 2012; Xu et al., 2016). Soil moisture limits gas transport, and it is often used as an implicit control on heterotrophic respiration and methanogenesis. However, the explicit processes resulting from soil oxygen depletion (e.g., soil redox status and pH dynamics)
25 are not widely represented (Riley et al., 2011; Meng et al., 2012).

The extent of SOM decomposition and gas emissions depends upon soil geochemical characteristics beyond temperature and O_2 availability. Among the wide range of environmental variables, pH emerges as a primary control on decomposition by regulating 30 both microbial communities and microbial metabolic activities (Zhalnina et al., 2015; Jin and Kirk, 2018). pH affects microbial metabolism by modulating the thermodynamics and kinetics of redox reactions. Redox reactions produce or consume protons, and thus, their free energy yields vary with pH (Bethke et al., 2011; Jin and Bethke, 2007). The Gibbs free energy available to anaerobic 35 microorganisms that degrade simple organic molecules generally increases (becomes less favorable) with increasing pH (Bethke et al., 2011). Notably, iron $[\text{Fe}(\text{III})]$ reduction is highly proton consuming and becomes less favorable at higher pH (Figure S1). Previous studies identified iron reduction as a major process in anoxic Arctic soils (Lipson et al., 2010; Lipson et al., 2013), which 40 increase local pH and might favor co-occurring methanogenesis (Tang et al., 2016; Wagner et al., 2017). However, the influence of iron reduction on methanogenesis rates in different soils is rarely investigated. The reactivity of iron and its pH-feedback impose additional complexity on the controls of SOM decomposition and associated CH_4 production.

Despite the importance of pH in controlling redox reactions and resulting C emissions, pH change, is not explicitly represented in 45 biogeochemical models. Most of the current biogeochemical models apply a single initial pH value for redox reactions without

Deleted: Disagreement in projections of the magnitude and timing of carbon release upon permafrost thaw could be due to differences in model structure, model initialization, or parameters used in simulations. Important geochemical and metabolic constraints might be poorly represented, oversimplified or missing in current biogeochemical models. To assess the impacts of geochemical constraints on projections of C emissions, we examine two mechanisms that substantially affect SOM turnover in permafrost-affected soils. First, rising temperature alters the kinetics of biogeochemical reactions (Segers, 1998). While temperature acts as an implicit control over permafrost SOM decomposition, the response to temperature rise is an empirical function that can vary for different processes (Treat et al., 2015; Koven et al., 2017). Microbial communities also change with temperature, compounding effects on process rates (Karhu et al., 2014). Models address this temperature effect using simplified response functions and parameters (Tuomi et al., 2008; Xu et al., 2016), which might be highly biased dependent upon model assumptions and original curve fitting techniques. Second, heterogeneity in permafrost thaw and related hydrological responses modulates decomposition rates and partitioning of CO_2 and CH_4 production

Deleted: Saturated conditions limit O_2 diffusion from the surface, favoring anaerobic respiration, fermentation,

Deleted: methanogenesis over aerobic respiration.

Deleted: , however,

Deleted: associated with oxygen depletion

Deleted: considered

Deleted: The fate of permafrost C is determined in large part by soil moisture, particularly water saturation caused by ice melting, precipitation, infiltration and runoff (Riley et al., 2011; Elberling et al., 2013; Schädel et al., 2016). Permafrost thaw frequently creates large areas of soil inundation due to abrupt surface collapse and subsidence (Painter et al., 2013; Walvoord and Kurylyk, 2016), resulting in higher levels of CH_4 production via anaerobic decomposition pathways. Although total carbon release under oxic conditions is much higher than under anoxic conditions (Schädel et al., 2016), emissions of high global warming potential CH_4 may offset this

Deleted: redox potential,

Deleted: simply considering

Deleted: concentrations. Thermodynamics predict that alternative electron acceptors such

Deleted: SO_4^{2-} , $\text{Fe}(\text{III})$ and NO_3^- could be favored over methanogenesis and drive C mineralization.

Deleted: (Bethke et al., 2011)

Deleted:)

Deleted: $\text{Fe}(\text{III})$

Deleted: can

Deleted: interaction with local soil geochemistry

Deleted: methanogenesis

Deleted: anaerobic SOM decomposition for predicting future climate change, it

Deleted: most

considering proton production and consumption during the processes. Traditional decomposition models use landscape position, soil moisture content, or other proxy of O₂ concentration to determine the form of C release. Scalars on aerobic respiration (Riley et al., 2011; Lawrence et al., 2015) or empirical ratios of CO₂ and CH₄ (Koven et al., 2015) are often used to inform the extent of C decomposition and partitioning of CO₂ and CH₄ production. Reactions that produce or consume protons and the resulting pH changes or ion exchange reactions are not considered in these empirical models. Some process rich models explicitly include details of methanogen populations and their interactions with substrates and other environmental factors, but these models still lack the capability to simulate pH changes during long-term carbon decomposition. Instead, constant pH is often assumed within bell-shaped pH response functions (Meng et al., 2012; Tian et al., 2010; Xu et al., 2015). Without underlying proton exchange and pH buffering mechanisms, a significant error may occur when rate calculations depend heavily upon the initial choice of a single optimal pH value for various reactions.

In this study we developed a new anaerobic carbon decomposition model framework with explicit representation of aqueous phase geochemistry to allow pH and thermodynamic calculations. By coupling three different models, including a thermodynamically based microbial growth model, a substrate pool-based model, and a humic ion-binding model, we built a process rich carbon decomposition model that allows simultaneous thermodynamic and pH calculations. Results from anoxic incubations of permafrost affected soils along a gradient of soil were synthesized to parameterize and validate this new model framework. The main objectives of this study were to (i) examine the role of soil geochemical variables in controlling anaerobic carbon decomposition and carbon release (as both CO₂ and CH₄); (ii) develop a common set of parameters in the new anaerobic carbon decomposition framework to capture variabilities in CO₂ and CH₄ production; and (iii) evaluate model uncertainties in responses to both soil heterogeneity and model parameterization, emphasizing effects of soil saturation, pH and temperature response.

2 Materials and methods

2.1 Site description and soil incubations

The Barrow Environmental Observatory (BEO) in Utqiagvik (Barrow) Alaska, USA consists of thaw lakes, drained thaw lake basins and interstitial tundra with a polygonal landscape of microtopographic features created by ice wedges. As part of the Next Generation Ecosystem Experiments Arctic project (<http://ngee-arctic.ornl.gov/>), frozen soil cores were collected from different microtopographic positions of Low-centered, Flat-centered, and High-centered polygons (LCP, FCP, HCP) in the wet tundra. LCPs are characterized by narrow, saturated troughs, raised rims, and wet, sometimes saturated centers (Figure 1) (French, 2007; Liljedahl et al., 2016). We previously performed short-term incubations of LCP soils under anoxic, environmentally relevant conditions to measure rates and temperature sensitivities of CO₂ and CH₄ production (Roy Chowdhury et al., 2015). FCPs represent transitional polygons with melting ice wedges, minimal rims, moderately dry centers, and disconnected troughs. Incubations of FCP soils demonstrated both methanogenesis and methane oxidation potential, with high levels of activity at the transition zone (Zheng et al., 2018). Finally, HCPs have well drained centers and low, saturated troughs. Incubations of HCP soils showed significant fermentation, methanogenesis and anaerobic respiration in the saturated troughs (Yang et al., 2016), contrasted with aerobic respiration and minimal methanogenesis in the centers (Roy Chowdhury et al., in preparation). These controlled incubations provided critical information on anaerobic SOM decomposition processes across a gradient of soil with fine-scale variability in thermal and hydrological regimes. The results facilitate benchmarking and parameterization for fine-scale anaerobic SOM decomposition models.

Deleted: The SOM decomposition regime is predominantly developed under aerobic respiratory conditions (Manzoni and Porporato, 2009). Current **Formatted:** Font: (Default) Cambria
Deleted: (Koven et al., 2015)
Deleted: However, methanogenesis and underlying anaerobic processes
Deleted: energetically different from aerobic respiration, generating large unresolved uncertainties.
Deleted: representation of aqueous chemistry reactions that would allow pH, redox potential and thermodynamic calculations (Segers and Leffelaar, 2001a, b; Segers et al., 2001; Xu et al., 2015; Grant, 1998, 1999).
Deleted: pH and redox potential are treated as status parameters in these models, and empirical
Deleted: are applied for simulations.
Deleted: and functional form
Deleted: In addition, the response of SOM decomposition to changes in temperature and moisture remains uncertain (Koven et al., 2017; Schädel et al., 2016). Regardless of modeling approach, the mathematical expressions for temperature or moisture responses vary among current decomposition models, and may not hold for anaerobic conditions since these relationships are mainly derived from aerobic processes. The lack of explicit anaerobic processes and aqueous chemistry in current biogeochemical models limits their predictive powers.
Deleted: .

Incubation datasets from 8 soil cores, divided in 126 soil microcosms associated with 14 treatments (soil microtopographic features \times soil layer) were included in this synthesis to represent the microtopographic heterogeneity of polygonal tundra. Soil cores were previously sectioned into organic, mineral, cryoturbated transition zone (if identified) and permafrost for microcosm incubations.

5 The period of anoxic incubation in these studies ranged from 45 to 90 days with an average of approximately 60 days at field-relevant temperatures of -2, +4 and +8 °C. Cumulative CO₂ and CH₄ production data were collected at different time intervals during incubations. More details on the microcosm construction, headspace CO₂ and CH₄ sampling, and rate calculations can be found in the corresponding publications (Roy Chowdhury et al., 2015; Herndon et al., 2015) and datasets (Zheng and Graham, 2017; Zheng et al., 2016). Changes in exchangeable Fe(II), water extractable organic carbon (WEOC), low molecular weight

10 organic acids, and pH of soil microcosms during anoxic incubation were summarized previously in publications (Herndon et al., 2015) and datasets (Zheng and Graham, 2017; Herndon et al., 2016).

2.2 Data processing and statistics

In order to compare the cumulative carbon loss (as both CO₂ and CH₄) from different polygonal and microtopographic features

15 and different soil layers, measurements from triplicate microcosms were pooled together and fitted with hyperbolic, sigmoidal, exponential or linear functions that best describe the dynamic. The cumulative CO₂ and CH₄ production within 60 days of anaerobic incubation was directly calculated from each fitted curve and used for descriptive statistical analyses.

Individual curve fitting for each microcosm was used to best represent the rate changes of CO₂ and CH₄ production. CO₂ production

20 followed hyperbolic curves with immediate CO₂ release for all LCP, FCP and HCP trough samples. CO₂ production from HCP center samples experienced time lags for approximately 10 days for the mineral layer, and 45 days for the permafrost. CH₄ production was also associated with varying time lags before reaching maximum rates, and the lag is most profound in HCP samples, between 6 to 20 days. The rate of gas production estimated from hyperbolic curve fitting predicts a continuously decreasing rate, while sigmoidal curve fitting with an initial delay predicts a maximum rate after the lag time. Here, we used the

25 derivatives of nonlinear curve fitting to calculate initial rates of gas production. For hyperbolic fittings, the maximum rate is calculated at day 0. For sigmoidal fittings, the maximum rate is calculated by setting the third derivative to zero. The temperature dependence was calculated using conventional Q₁₀ by taking the ratio of maximum production rates at 8 and -2°C based on triplicate measurements. Data fitting and statistical analyses were conducted and validated using R 3.4.0 (The R Foundation for Statistical Computing) and Python 3.6.0 (Python Software Foundation) computing environments. A complete list of packages and libraries

30 used here can be found in the following references (Venables and Ripley, 2002; Hunter, 2007; Oliphant, 2007; Sarkar, 2008; Walt et al., 2011; Wickham, 2009; Wickham et al., 2017).

2.3 Anaerobic carbon decomposition model

The anaerobic carbon decomposition framework was developed with explicit representation of fermentation, methanogenesis and iron reduction, which were identified as key mechanisms for anaerobic CO₂ and CH₄ production (Roy Chowdhury et al., 2015; Yang et al., 2016; Zheng et al., 2018). The main structure of this framework included two major components: a simplified CLM-CN decomposition cascade (Converging Trophic Cascade, or CTC) (Thornton and Rosenbloom, 2005) to facilitate parameterization of the upstream carbon flow entering aqueous phase dissolved organic carbon (DOC) pool (Figure 1, process 1), and an aqueous phase to facilitate calculations of thermodynamics and redox-reaction associated acid-base chemistry. An empirical

Deleted: The anaerobic carbon decomposition framework was developed with explicit representation of fermentation, methanogenesis and iron reduction, which were identified as key mechanisms for anaerobic CO₂ and CH₄ production (Roy Chowdhury et al., 2015; Yang et al., 2016; Zheng et al., 2018). We used a thermodynamically-based approach (Istok et al., 2010) to represent methanogenesis and iron reduction, with unique microbial growth kinetics incorporated into energy yielding redox reactions. An aqueous phase was introduced into the model to facilitate thermodynamic calculation and redox-reaction associated acid-base chemistry calculation. Proton exchange was provided by SOM using a humic ion-binding model (Tipping, 1994; Tipping, 1998), allowing calculation of pH dynamic during anaerobic carbon decomposition. Given the difficulties in partitioning SOC into chemically distinct pools, the CLM-CN decomposition cascade (Converging Trophic Cascade) was adopted to simulate discontinuous carbon pools with different complexity (Thornton & Rosenbloom, 2005, Tang et al., 2016, Xu et al., 2015) and to facilitate parameterization of the upstream carbon flow entering aqueous phase dissolved organic carbon (DOC) pool (Figure 2, process 1). The above model structure was implemented into the open source geochemical model PHREEQC (Charlton & Parkhurst, 2011).

Moved down [1]: A temperature effect was parameterized using the CLM-CN temperature response function (Appendix B, equation B1).

approach was used to represent non-aqueous phase SOC decomposition, while mechanistic representation of methanogenesis and iron reduction were developed in this work based on aqueous phase thermodynamic calculations.

The simplified CTC cascade included 4 SOM pools to represent bulk SOC with different levels of complexity. Changes of these 5 SOM pools followed modified first-order-decay (see Supplementary Material for details). We modified the original respiration fraction (Thornton and Rosenbloom, 2005; Koven et al., 2013) into a direct and an indirect fraction. Thus for each SOM pool, the direction respiration fraction represented CO_2 lost as originally defined, while the indirect respiration fraction was labile C produced from bulk C entering the aqueous phase carbon pool (DOC pool, Figure 1).

10 The large biomolecules in the DOC pool went through multiple hydrolysis and fermentation steps to produce low molecular weight organic acids that would further respire into CO_2 and CH_4 (Kotsyurbenko, 2005; Yang et al., 2016). Under anoxic conditions, hydrolysis of polysaccharides was considered the rate-limiting step for downstream methanogenesis (Glissmann and Conrad, 2002). Polysaccharide hydrolysis has a favorable free energy, due to increased entropy, but cannot be readily coupled to biological energy transduction outside of the cell. At low temperature (below 15 °C), the microbial degradation of cellulose was considerably 15 diminished while other polymers, such as starch or proteins, were degraded much faster at low temperature, resulting in the accumulation of organic acids, primarily acetic, propionic and butyric acids (Kotsyurbenko, 2005; Yang et al., 2016). These low molecular weight organic acids further fueled microbial mineralization reactions that lead to production of CH_4 and CO_2 . Given that most anaerobic lignocellulose degraders also fermented sugars following hydrolysis (Blumer-Schuette et al., 2014), we assumed the turnover of DOC into low molecular weight organic acids was a single lumped fermentation process (Figure 1, process 20 2), in which labile DOC ($\text{C}_6\text{H}_{12}\text{O}_6$) was fermented into acetate, H_2 and CO_2 (Appendix A, reaction A1). This assumption gave a fixed stoichiometry ratio that 1/3 of the fermented carbon was respired as CO_2 .

25 Redox reactions including methanogenesis and iron reduction were represented using a thermodynamically-based approach (Istok et al., 2010), with unique microbial growth kinetics incorporated into energy yielding redox reactions. In this thermodynamically based approach, the growth equations of methanogens and iron reducers were derived from paired electron donor (acetate and H_2) and electron acceptor half reactions and a biomass synthesis equation (Istok et al., 2010). Using a constant molecular formula as biomass ($\text{C}_6\text{H}_{12}\text{O}_6\text{N}$), and ammonium (NH_4^+) as the nitrogen source for biosynthesis, we derived the growth equations for methanogenesis and iron reduction (Appendix A, equation A2-A5). Rate calculations followed the generalized Monod rate law (Jin and Bethke, 2007) with an additional thermodynamic factor representing the thermodynamic driving force. The 30 thermodynamic factor $f(G)$ is calculated using equation 1 (Jin and Bethke, 2003):

$$f(G) = 1 - \exp \left(-\frac{\Delta G - m\Delta G_p}{\chi RT} \right) \quad (1)$$

where ΔG [kJ (mol reaction) $^{-1}$] is the free energy change of the redox reaction [ΔG depends on the standard Gibbs free energy change (ΔG^0), and the concentrations of chemical species involved in the reaction], and ΔG_p is the phosphorylation potential, i.e., 35 the energy required to synthesize ATP to ADP and dihydrogen phosphate in cell's cytoplasm. ΔG_p is about 45 kJ (mol ATP) $^{-1}$ (Jin and Kirk, 2018). m is the number of ATPs synthesized per redox reaction. χ is the average stoichiometric number (Jin and Kirk, 2018). R is the gas constant (kJ mol $^{-1}$ K $^{-1}$), and T is the absolute temperature (K). This factor $f(G)$ ranges from 0 to 1, where the reaction is thermodynamically favorable when $f(G) > 0$.

40 Both methanogenesis and iron reduction contribute to pH change. Reactions such as ferrihydrite reduction substantially increase

Deleted: 1

Under anoxic conditions, the hydrolysis of polysaccharides is considered the rate-limiting step for downstream methanogenesis (Glissmann and Conrad, 2002). The microbial degradation of cellulose is considerably diminished at low temperature (below 15 °C), while other polysaccharides, such as starch, or proteins are degraded much faster at low temperature, resulting in the accumulation of organic acids, primarily acetic, propionic and butyric acids

Formatted: Font: Font color: Black

Deleted: . These polymers are degraded through several hydrolysis and fermentation steps to produce highly biodegradable low molecular weight organic acids that fuel microbial mineralization reactions, leading to production of CH_4 and CO_2 . Instead of including multiple hydrolysis and fermentation steps, we assumed the turnover of DOC into low molecular weight organic acids is a single lumped fermentation process (Figure 2, process 2). Most anaerobic lignocellulose degraders also ferment sugars following hydrolysis, justifying this assumption (Blumer-Schuette et al., 2014). 1

Formatted: Font: (Intl) Arial Unicode MS

Deleted: that consume or produce protons are sensitive to pH.

Formatted: Font: Font color: Text 1

alkalinity (Appendix A, Reaction A4, A6). Furthermore, the solubility of CO₂ and the composition of dissolved CO₂ and bicarbonate vary significantly over typical soil pH values, affecting all C mineralization processes. In the organic-rich soils modeled here, SOM rather than minerals provides most buffering capacity. Therefore, we used the humic ion-binding model to describe pH buffering during carbon decomposition. A simplified parameterization of proton binding is available in the Windermere Humic Aqueous Model (WHAM, Tipping, 1994; Tipping, 1998), which has been extensively calibrated to represent the acid-base chemistry of “average” humic and fulvic acids, and benchmarked with heterogeneous natural organic matter (Atalay et al., 2009). We adopted the WHAM parameterization to represent proton binding characteristics (pH buffering) provided by SOM (Tang et al., 2016). Using representative binding constants provided by WHAM, the pH buffering capacity can be directly adjusted by altering the number of proton binding sites, which is assumed to be linearly correlated with total amount of SOM (see 10 [Supplementary Material for details](#)).

Deleted: The humic ion-binding model calculates chemical equilibrium using strong or weak binding sites of organic matter with various proton binding constants (Dudal & Gérard, 2004).

Deleted: it was

Deleted: (Atalay et al., 2009), we

Deleted: pH buffering

Deleted: SOM. Therefore

2.2 Model implementation and initialization

The above model structure was implemented using the open source geochemical program PHREEQC 3.0 (Charlton & Parkhurst, 2011) with a new database describing SOC decomposition cascade, redox reaction kinetics and pH buffering (*redox.dat*, available at <https://github.com/jianqizh/decomposition>). The model assumed thermodynamic equilibrium of aqueous chemical speciation, mineral dissolution/precipitation, and ion sorption/desorption based on the updated PHREEQC thermodynamic database (*phreeqc.dat*, Charlton & Parkhurst, 2011). The database was modified to include WHAM pH buffering and reaction kinetics for SOM pools decay and reaction kinetics for fermentation, methanogenesis and iron reduction. The kinetic rate 20 constants and microbial biomass growth and decay rates were adopted from former thermodynamically based studies (Istok et al., 2010) and pre-tested with low-center polygon Arctic soils (Tang et al., 2016).

The model initialization was based on both the incubation conditions and soil geochemical characterizations (Figure S2). The initial partitioning of SOM pools was assumed to be at fixed ratios due to the limitation of short-term incubation data. Under the 25 experimental conditions, we assumed SOM1 and SOM2 pools with relatively shorter turnover rate ($\tau = 14$ days and 70 days, respectively) were most relevant in the model, while SOM3 and SOM4 ($\tau > 2$ years for both pools) pools were relatively inert. We started with the relative fraction of SOM pools at approximately 10%, 40%, 10% and 40% of SOC in organic and mineral soils for SOM1-4 pools and further assessed the bias of this assumption with sensitivity analysis. Sizes of SOM1 and SOM2 pools were reduced by 90% for permafrost to better account for the overall low levels of carbon degradation in soils at such depth.

30 All other variables required were initialized using measurements based upon 10 to 15 g of wet soil incubated in 60 to 70-mL sealed bottles. Total soil organic carbon (SOC), total water (TOTW), total organic acid carbon (TOAC), pH and initial concentration of Fe(II) were specified in the model based on measurements (Table S1). The DOC pool in the model was initialized using the measured WEOC expressed as a fraction of SOC (f_{doc}). On average, WEOC accounts for approximately 2% of SOC based on our 35 synthesized data (see section 3.1), consistent with previous long term incubations, which suggested less than 5% of SOC were fast decomposing carbon in permafrost affected soils at a standardized temperature of 4-5 °C (Knoblauch et al., 2013; Schädel et al., 2014). The starting biomass of methanogens and iron reducers was assumed to be within the range of 10^{-3} to 10^{-5} gC/gSOC for organic soils, 10^{-4} to 10^{-6} gC/gSOC for mineral soils, and 10^{-7} to 10^{-9} gC/gSOC for permafrost (Table S1). This stratified microbial biomass distribution were used to represent the vertical gradient in the relative abundance of microbial communities (Treat et al., 40 2014; Waldrop et al., 2010; Yang et al., 2017).

Deleted: . The influence

Moved (insertion) [2]

The lumped fermentation process was the rate-limiting step in the model and was fitted individually with data from each soil microcosm. Based upon reaction stoichiometry, the fermentative conversion of each mole of labile C led to 2/3 mole of organic acids and 1/3 mole of CO₂. Organic acids were mineralized via methanogenesis or iron reduction to convert approximately 49% to 88% of C in organic acids into CO₂. This estimation was based on reaction stoichiometry of A2 and A4, and a fraction of the C was incorporated into microbial biomass, so the percentage of respired C would be less than 100% even if all organic acids were respired as CO₂. If we assume all fermentation products were mineralized into CH₄ and CO₂, we could estimate the fermentation rate (R_{fer}) from measured CO₂ production. Thus, R_{fer} were estimated using the initial CO₂ production rate in the incubation data, and further optimized by fitting with observed CO₂ production.

10

Temperature and pH response functions were used to further constrain model simulations (Figure S2). A temperature effect was parameterized using the CLM-CN temperature response function (Appendix B, equation B1). Additional temperature response functions were evaluated by sensitivity analysis (see section 2.4). The effect of pH on biological reaction rates is modulated by bell-shaped pH response functions (Tang et al., 2016; Xu et al., 2016). Here we used the Dynamic Land Ecosystem Model (DLEM) pH response function (Appendix B, equation B5), since it generates the least variation in parameter perturbation tests (Tang et al., 2016).

15

2.3 Incubation data synthesis for model validation

Incubation data from Utqiagvik (Barrow) Alaska soil cores that represent the microtopographic heterogeneity of polygona tundra were synthesized to validate the new anaerobic carbon decomposition model. The selected datasets represent fine scale variabilities in thermal and hydrological regimes across the gradient of soil microtopographic positions (Herndon et al., 2015). The synthesized data contains complete sets of soil geochemical descriptions for organic, mineral, transition zone (if identified) and permafrost layers from each microtopographic feature (see Supplementary Material for details). Levels of total soil organic carbon, water extractable organic carbon (WEOC) and total organic acid carbon (TOAC) were available before and after soil incubation. Besides CH₄ and CO₂ production during low temperature soil decomposition, data on Fe(II) concentrations and pH changes were also available for model initialization and validation.

20

2.4 Model parameter uncertainty

This model is designed as a generic framework to simulate anaerobic carbon decomposition across a range of soil physiochemical conditions. Two types of sensitivity analysis were conducted to evaluate model performance. First, possible bias and variations associated with model initialization variables (soil geochemical attributes) were assessed using perturbation simulations. Variations of $\pm 25\%$ and $\pm 50\%$ (+100% and 200% for some variables) were applied to these variables, and the resulting changes in cumulative CO₂ and CH₄ production were evaluated by comparing with reference simulations. This evaluation helps to identify critical measurements needed for initializing the model. Second, parameters specifically benchmarked in this study and parameters adopted from empirical relationships were also evaluated with perturbation simulations. This test helps to apportion the model prediction uncertainties into different sources, including model input, parameters, or model structure.

3 Results

Moved (insertion) [1]

Deleted:

Deleted: with a single optimal value between pH 5 to 7

Deleted: The

Deleted:) is used in this model

Field Code Changed

Deleted: 2.4 Model initialization and

Deleted: In this anaerobic carbon decomposition framework, we focused on developing and validating parameters for anaerobic mechanisms leading to CO₂ and CH₄ production. The kinetic rate constant and microbial biomass growth and decay rates were adopted from former thermodynamically based studies (Istok et al., 2010). Previous long term incubation studies suggest the size of the fast carbon pool is less than 5% of SOC in permafrost affected soils, with a mean turnover rate (τ) between 77 to 150 days at standardized temperature (4-5 °C)

Moved up [2]: (Knoblauch et al., 2013; Schädel et al., 2014).

Deleted: This turnover rate is most relevant to SOM1 ($\tau=14$ days) and SOM2 ($\tau=70$ days) in the decomposition model (Thornton & Rosenbloom, 2005; Tang et al., 2016; Xu et al., 2015), thus we start with 1% and 4% of SOC as the initial values of SOM1 and SOM2. Therefore, a lumped fermentation process was assumed to represent the turnover of DOC into low molecular weight organic acids. The fermentation rate can be directly estimated from CO₂ production based upon reaction stoichiometry of fermentative conversion of glucose into acetate and further decomposed via acetotrophic methanogenesis or Fe(III) reduction (Appendix A). The maximal production of CO₂ is about 2/3 of the initial carbon. Thus, the fermentation rate (R_{fer}) is estimated using the initial CO₂ production rate in the incubation experiment and further optimized by fitting with observed CO₂ production.¶

The model was initialized using measurements based upon 10 to 15 g of wet soil incubated in 60 to 70-mL sealed bottles. Total soil organic carbon (SOC), total water (TOTW), total organic acid carbon (TOAC), pH and initial concentration of Fe(II) were specified in the model based on measurements. The DOC pool in the model was initialized using the measured WEOC, and expressed as a fraction of SOC (f_{doc}) (Table S2). The starting biomass of methanogens and iron reducers was assumed to be in the range of 10^{-4} to 10^{-7} gC/gSOC and further adjusted to fit the observations. Model fitted fermentation rates are summarized in Table S3.¶

3.1 Meta-analysis to validate model assumptions

Incubation data used in this study were generated from soils representing different microtopographic features with a wide range of moisture and SOC contents and reported elsewhere (Roy Chowdhury et al., 2015; Zheng et al., 2018). Correlation analysis revealed a close relationship between soil moisture and organic carbon pools (measured as SOC, WEOC and TOAC) among examined soil microtopographic features and across soil depth ($p < 0.01$, Table S2). All these soil properties showed significant correlation with cumulative CO_2 and CH_4 production ($p < 0.05$), suggesting the important role of initial soil geochemical properties in controlling carbon degradation.

Although various levels of carbon mineralization were measured as CO_2 and CH_4 production during incubations, changes in WEOC and TOAC were consistent among treatments with distinct patterns. WEOC represents 0.3% to 2.6% of total SOC among all test soils, and this ratio remained constant before and after anoxic incubations (Figure S3). On the other hand, TOAC showed much more dynamic changes among different soils and different incubation temperatures. TOAC generally increased in soils from organic layer, transition zone and permafrost. In contrast, TOAC drastically decreased by up to 90% in mineral soils. These results indicate that WEOC was in a steady state among examined soils, while TOAC varied substantially due to microbial mineralization processes, supporting the model assumptions of lumped fermentation (the conversion of WEOC to TOAC) as rate limiting step.

Both CO_2 and CH_4 production rates responded strongly to rising incubation temperature ($p=0.02$ and $p=0.04$, respectively, Figure S4, Table S3). The estimated Q_{10} values of CO_2 production showed a relatively narrow range while methanogenesis had much larger variations in estimated Q_{10} values ranging from 1.6 to 48.1. Using Q_{10} values to simulate the temperature dependence of processes might work for CO_2 production, but could generate significant errors in predicting CH_4 production.

3.2 Modeled CO_2 and CH_4 production using observed parameters

The model performed well in simulating CO_2 and CH_4 dynamics across a range of moisture and SOC gradients and among different soil types (Figure S5, S6). Variations in gas production among different conditions, including microtopographic features, soil layer, and different incubation temperatures were well captured (Figure S7). The comparisons between modeled and observed CO_2 and CH_4 production are shown in Figure 2. The model slightly underestimates CO_2 production towards the end of the incubations, but still maintains a good agreement between modeled and observed CO_2 production ($R^2=0.89$). The underestimation of CO_2 production is likely due to substrate limitations caused by the initial distribution of different carbon pools. Model-predicted CH_4 production also showed good agreement with observations ($R^2=0.79$). More variation between modeled and observed CH_4 production suggests a systematic pattern in the model parameterization of methanogenesis: the model underestimates CH_4 production at 4 and 8°C, and overestimates CH_4 production at -2°C.

To assess the model sensitivity to initial model inputs, we compared model predictions in response to varying initial model inputs via perturbation simulations. First, we examined the influence of the partitioning of different carbon pools. Significant changes in model predictions of CO_2 and CH_4 were observed in response to perturbations of initial input of SOC, WEOC, but not TOAC (Figure 3). SOC determines the size of different carbon pools in the model, and it further influences the predictions of WEOC, TOAC, CO_2 and CH_4 . For example, predicted CO_2 and CH_4 production increased by about 200% when +200% changes were applied to initial SOC input. This trend is consistent with correlation analysis of incubation results described above (Table S2).

Deleted: 3.1 Synthesized soil geochemical characteristics
Soil samples
Deleted: represent
Deleted: content, from 2% to 39%, with the highest SOC found in surface
Deleted: layers. In correlation analysis
Deleted: characteristics, both WEOC and TOAC showed strong correlation with SOC content among examined soil cores and across soil depth (Table 1). Decomposition generated limited
Deleted: .
Deleted: 26
Deleted: 3a). Higher incubation temperatures showed minimal effect on the WEOC/SOC quotient, and a ... [2]
Deleted: by 5% to 175%
Deleted: soils, and 2% to 60% in the
Deleted: from LCP and HCP centers (Figure 3b). In most
Deleted: %, partially contributing to the depletion of ... [4]
Deleted: usually
Deleted: activity
Deleted: Good correlations between soil organic carbon [5]
Formatted: Font: Not Bold, (Intl) Arial Unicode MS
Deleted: ,
Formatted: Font: Not Bold, (Intl) Arial Unicode MS
Deleted: response and soil layer effects ... [6]
Deleted: <0.001 and $p < 0.001$, respectively, Figure 4) ... [7]
Deleted:). A significant temperature \times soil layer ... [8]
Formatted ... [9]
Deleted: value was calculated for each condition to further ... [10]
Deleted: between 4.6 and 5.0. Mineral soils with lower ... [11]
Deleted: . Organic soils had a Q_{10} value between 18.5 and
Deleted: , while in mineral soils and permafrost, the ... [12]
Formatted ... [13]
Deleted: 1 ... [14]
Formatted ... [15]
Deleted: 3
Deleted: 5
Deleted: maintain
Deleted: The
Deleted: .
Deleted: and moisture
Deleted: 6
Deleted: , which
Deleted: our synthesis
Deleted: 1

Perturbations in initial WEOC strongly altered the predictions of TOAC and CO₂, consistent with the model assumption of the conversion of WEOC to TOAC (fermentation process) as the rate-limiting step. The model also predicted increases in CH₄ and Fe(II) accumulation in response to lower WEOC. Lower WEOC significantly reduced organic acid accumulation, and thus, increased system pH and accelerated rates of both methanogenesis and iron reduction. The starting level of TOAC showed minimal 5 influence on model predictions of CO₂ and CH₄, suggesting other factors rather than substrate availability were limiting carbon mineralization. The initial sizes of SOM1 and SOM2 pools showed very slight changes in model predictions of WEOC and CO₂, and minimal influence on CH₄ prediction, further justifying downstream fermentation process as rate-limiting step in the model. Additional soil geochemical factors, including soil moisture, Fe(II) and pH also significantly influence model output. In particular, initial soil pH showed a dramatic effect on predicted CO₂ and CH₄ production. With initial soil pH increased from 5 (reference 10 simulation) to 6, the model predicted 160% and 308% increase in CO₂ and CH₄ production, respectively. Perturbations in initial soil pH had the strongest effect on the prediction of CH₄ by assigning different values in f_{pH} that were directly proportional to the methanogenesis rates. The above results of perturbation simulations demonstrated high sensitivity of this model in response to varying soil geochemical properties.

15 3.3 Model sensitivity to parameterization uncertainties

To further validate the model, we performed additional sensitivity analysis to justify model assumptions and estimate the uncertainties generated from model parameterizations. One major assumption of this modeling framework is to lump multiple fermentation processes into one reaction stoichiometry, controlled by one reaction rate constant. It is critical to evaluate how this simplified structure influences model performance and contributes to model output uncertainties. The model parameter sensitivity 20 analysis indicated the TOAC pool was most sensitive to changes in the fermentation rate (R_{fer}) and reaction stoichiometry (Figure 4). Downstream reactions were less affected by the uncertainties of the two tested parameters. These results supported our assumption of lumped fermentation with fixed stoichiometry, indicating the robustness of the model structure presented here.

The selection of temperature response functions represents one of the major sources of model uncertainties. A sensitivity analysis 25 was performed by comparing four different temperature response functions (Appendix B). In our simulations, the quadratic temperature response function proposed by Ratkowsky et al. predicted much higher CO₂ and CH₄ production rates at higher temperature, and the lowest rate of both CO₂ and CH₄ at temperatures below 0 °C, giving the highest temperature response among tested response functions (Figure 5). In contrast, the Arrhenius equation predicted much lower temperature response for both CO₂ and CH₄. Empirical functions used in CLM-CN and CENTURY gave similar temperature response for both CO₂ and CH₄. 30 Variations in low temperature CO₂ production is well constrained by established temperature response functions, while CH₄ production at -2 °C showed a much wider range of temperature response, and the median value is best simulated using Ratkowsky function. This sensitivity analysis is consistent with model output of CO₂ and CH₄ production, where CO₂ is well constrained by the model, but CH₄ is significantly overestimated at -2°C using CLM-CN temperature response function. A unified temperature response function for all reactions under different biotic or abiotic constraints substantially contributes to the disagreement between 35 model output and observations.

Redox reactions contribute to proton production or consumption, and the resulting pH alters the value of the pH response function (f_{pH}) that directly controls reaction kinetic functions, creating a feedback loop. pH buffering capacity (BC) provided by SOM with proton binding sites and f_{pH} represent two major sources of uncertainties in this feedback loop. Thus, we performed perturbation

Deleted: influence
Deleted: WEOC,
Deleted: as one of the major assumptions of
Deleted: is that
Deleted: is
Deleted: dramatic
Deleted: , which is related to pH response of methanogenesis and Fe(III) reduction.

Deleted: : an increase in pH from 4.92 to 5.15 to 6.14 was predicted in the model when initial WEOC was adjusted 25% or 50% lower, respectively. This drastic pH change is consistent with observations that pH increased up to 1 pH unit during short-term incubations (Roy Chowdhury *et al.*, 2015). Simulated pH increase represented 54% and 354% increases in the value of the pH response function (f_{pH}), which substantially

Deleted: Similarly, perturbations
Deleted: initial reaction

Deleted: 4

Deleted: One of
Deleted: assumptions

Deleted: 7

Deleted: on temperature response
Deleted: with

Deleted: 8

Deleted: pH response function

simulations to characterize the sensitivity of model output to variations in BC and f_{pH} (Figure 6). Higher BC stabilized system pH during prolonged incubations, while lower BC permitted a pH increase by up to 0.71 pH unit compared to the reference simulation. This 14% pH increase led to a 123% increase in f_{pH} , accelerating both methanogenesis and Fe(III) reduction rates substantially. Perturbations on pH response function were directly reflected in the slopes of pH response curves (Figure S8). We found up to 5 372% change in the value of f_{pH} during a 60-day simulation, as steeper increase in f_{pH} accelerated both methanogenesis and iron reduction (equation A2-A5), which contributed to pH rise in the loop, further accelerating f_{pH} increase. Correspondingly, both CH₄ and Fe(II) increased by more than 100% after the simulation. While BC is an important factor controlling both redox reactions and pH fluctuations, a unified *fit* for all reactions may impose significant variations in model output.

Deleted: pH buffering capacity
Deleted: 9
Deleted: pH buffering capacity
Deleted: pH buffering capacity

10 BC is an intrinsic soil property simulated with a simplified linear relationship to soil SOM. However, it generates strong nonlinear response in the simulations of methanogenesis and Fe(III) reduction (Figure 7a). Simulations with varying soil BC revealed dynamic pH change at lower BC (Figures 8 and 9, with BC=1 as reference simulation), and stabilized pH at higher BC. At constant temperature, rates of both methanogenesis and Fe(III) reduction increased significantly at lower BC due to pH control. At lower BC when pH change is not well buffered, higher pH accelerated CH₄ and Fe(II) production rates (Figure 7), giving much higher 15 apparent temperature responses, while at higher BC with stabilized pH in the system, apparent temperature responses of these redox processes were significantly lower than the reference simulation (BC=1). Variations in pH buffering capacity generated large variations in apparent temperature responses of methanogenesis and Fe(III) reduction due to the pH feedback loop.

Deleted: pH buffering capacity
Deleted: pH response function

Deleted: Soil pH buffering capacity
Deleted: 9a
Deleted: buffering capacity (BC)
Deleted: Figure 9a, Figure 10c
Deleted: 10

4 Discussion

4.1 Synthesized soil geochemistry and model validation

20 Soil geochemical characteristics represent important abiotic controls on anaerobic carbon decomposition and subsequent CO₂ and CH₄ production. SOC content, soil pH, water table position, C:N ratio, and landscape position were all suggested to contribute to the variability in anaerobic CO₂ and CH₄ production (Lee et al., 2012; Schädel et al., 2014; Treat et al., 2015). We synthesized incubation data for gelisol soils from different pedons and soil moisture regimes representing heterogeneity across the BEO. This coordinated data set allowed us to focus on individual factors and their roles in relation to anaerobic CO₂ and CH₄ production.

25 Carbon released as CO₂ and CH₄ during anoxic incubations decreased with depth. Permafrost was associated with low levels of CO₂ production and very low CH₄ production, consistent with a previous synthesis (Treat et al., 2015). Nevertheless, permafrost TOAC, WEOC, and SOC concentrations were all comparable to organic soils, suggesting high substrate availability but low microbial activity. This trend is consistent with previous studies (Walz et al., 2017; Treat et al., 2015), where highest microbial 30 abundance and diversity were observed in surface soil and permafrost contained low microbial abundance (Treat et al., 2014; Waldrop et al., 2010). Among surface soils, higher moisture in low-centered polygon soils significantly promoted CO₂ and CH₄ production and the accumulation of fermentation products (measured as TOAC), emphasizing the importance of soil SOC content and moisture as strong environmental drivers for carbon decomposition. Given the bias in correlation analysis created by the skewed distribution of CO₂ and CH₄ production in our dataset, additional cluster analysis was performed based on data similarity 35 rather than correlations. High similarity of soil attributes (depth, moisture, pH, C:N ratio, SOC, TOAC) with CH₄ production (Figure 8a) was found, suggesting methanogenesis is potentially controlled by a set of soil geochemical characteristics in the local microenvironment.

Deleted: (Treat et al., 2015)

Deleted: ,
Deleted: ,
Deleted: LCP
Deleted: , Figure 3
Deleted: (Table S1, Figure S2).

Deleted: 11a

These synthesized observations support the major assumptions of our model development: (1) the [coupled hydrolysis and fermentation processes](#), converting macromolecular SOM into low molecular weight organic acids is the rate limiting step; (2) different rates of CO₂ and CH₄ production from different soil layers can be attributed to variations in microbial activity manifested as differences in initial microbial biomass or growth rates. Additional observations of substantial Fe(III) reduction and associated pH increases during anaerobic decomposition (Figure S9) confirmed the need to simulate pH variations associated with redox reactions and corresponding microbial responses. This anaerobic carbon decomposition framework adequately modulated the involved biotic and abiotic interactions by splitting the carbon flow to different redox reactions and simulating pH buffering capacity to mediate associated changes in acidity or alkalinity.

10

The model presented here identified fermentation, acetotrophic methanogenesis and acetotrophic iron reduction as key mechanisms for anaerobic CO₂ and CH₄ production (Vaughn et al., 2016; Lipson et al., 2010). Although denitrification, ammonification and sulfate reduction are all thermodynamically more favorable, low nitrate and sulfate concentrations in BEO soils limit flux through these pathways (Newman et al., 2015). We performed another cluster analysis on the model output (Figure 8b), where we not only simulated fermentation, methanogenesis and iron reduction rates and associated pH changes, but also tracked the biomass of methanogens (M_Meb) and iron reducers (M_Feb). A dendrogram depicting data similarity showed four distinct clusters comprising of WEOC, CO₂ (CO₂ prediction), Ferrous (Fe(II) prediction), and CH₄ (CH₄ prediction) that closely associated with soil geochemical properties and incubation temperature. This result is similar to the cluster analysis of synthesized data, further validating the proposed model structure in capturing major relationships between carbon mineralization and soil geochemical attributes. Predicted CH₄ production is strongly influenced by incubation temperature, soil pH, and soil moisture and depth that determines the size of methanogen population. This model prediction is consistent with previous studies on the vertical distribution of methanogen population (Waldrop et al., 2010). Environmental factors, such as labile organic matter, water table depth, and soil redox status, soil alkalinity and salinity (Wachinger et al., 2000; Rivkina et al., 2007; Høj et al., 2006; Yang et al., 2017) are all likely to contribute to the variabilities in the distribution and abundance of methanogens and subsequent methane production.

25 4.2 Temperature and pH response of anaerobic carbon decomposition

Rising temperature promotes anaerobic carbon decomposition, resulting in increased rates of anaerobic CO₂ and CH₄ production (Treat et al., 2014; Lupascu et al., 2012). It is widely recognized that methanogenesis is more sensitive to temperature than respiration (Yvon-Durocher et al., 2014; Yvon-Durocher et al., 2012), and it is usually associated with large variations. Segers estimated the Q₁₀ value of methanogenesis ranged from 1.5 to 28 among 1043 incubation experiments using wetland soils (Segers, 1998). Our data synthesis revealed even higher temperature sensitivity than other reported values. High estimated temperature sensitivity across the freezing point of water has previously been documented (Waldrop et al., 2010) and further attributed to limited water availability for microbial activities at sub-zero temperature (Tilston et al., 2010). Ratkowsky et al. proposed a quadratic relationship for the temperature dependence of microbial growth rates that modeled low-temperature growth better than the Arrhenius Law (Ratkowsky et al., 1982). Our simulations suggest better prediction of methanogenesis with this temperature response function, possibly due to a more suitable representation of growth limitation of methanogens at sub-zero temperature. Methanogenesis rates are also influenced by the availability of alternative electron acceptors and carbon source. Processes contributing to the accumulation or consumption of carbon substrates and competing electron acceptors may respond differently to temperature change, which could further complicate the temperature sensitivity of methanogenesis. Current modeling approaches heavily depend upon empirical temperature response functions, which may be associated with large uncertainties due

Deleted: process

Deleted: (Newman et al., 2015).

Deleted: 11b

Deleted: (Waldrop et al., 2010)

Formatted: Font: Not Bold

Formatted: Font: Not Bold

Deleted: (Segers, 1998)

Deleted: (Waldrop et al., 2010)

Deleted: (Tilston et al., 2010)

Deleted: (Ratkowsky et al., 1982)

to variations in the selection of data and curve fitting methods. Extrapolation of carbon decomposition rates, particularly methanogenesis rates, into a future warmer climate remains uncertain. More accurate simulations will require additional information on geochemical properties that contribute to the variations of methanogens distribution and methanogenesis activity.

5 pH values impose fundamental physiological restrictions on microbial activities. Soil pH ranges from acidic to circumneutral (pH 4-7.5) in northern Alaska and varies substantially through the soil profile and along the microtopographic gradient. Accumulation of organic acids in anoxic soils leads to pH decline (Jones et al., 2003), while consumption of organic acids by methanogenesis and iron reduction increases the alkalinity of the system via the production of HCO_3^- and OH^- (Drake et al., 2015; Roy Chowdhury et al., 2015; Howell et al., 1998). The interplay of these processes leads to strong nonlinear pH feedbacks in the system, and 10 previous studies have observed up to 1-2 pH unit changes during short-term anoxic incubations (Xu et al., 2015; Drake et al., 2015; Roy Chowdhury et al., 2015). These relationships between pH and organic carbon decomposition can vary in sign and magnitude. Our model simulations with mechanistic pH evolution indicate that constant pH assumed in previous models may cause significant 15 errors in simulating long-term anaerobic CO_2 and CH_4 production. The intrinsic soil pH buffering capacity plays a large role in stabilizing soil pH and may vary depending upon solution acidity or alkalinity, cation exchange capacity, SOM content and mineral composition and/or dissolution. These properties derive from SOM characteristics, moisture, mineral content, and additional geochemical properties, leading to complex correlations between soil pH and SOC decomposition rate that require future investigation.

4.3 Fast-decomposing carbon pool

20 Substrate availability is a primary determinant of potential CO_2 and CH_4 production (Lee et al., 2012; Schuur et al., 2015; Tarnocai et al., 2009). Total SOC is composed of heterogeneous C pools characterized by different turnover times. Carbon release during short term incubation originates from the C pool with relatively rapid turnover. The size and turnover time of this quickly-metabolized carbon pool is usually estimated by two-pool or three-pool conceptual models with a maximum likelihood solution 25 using time series of CO_2 data (Schädel et al., 2013). A previous study on Siberian permafrost soils using a two-pool model estimated a turnover time of 0.26 years for the fastest-responding pool (Knoblauch et al., 2013). A three-pool model was applied using more extensive incubation datasets collected from 23 high-latitude ecosystems, yielding an estimate of 0.35 years mean turnover time for the fastest-responding carbon pool (Schädel et al., 2014).

30 In our synthesis study, we directly quantified WEOC and assumed it represented the fast-decomposing labile carbon pool. The size of the labile carbon pool is constant during anaerobic decomposition, while total CO_2 and CH_4 release represent up to 194% of the labile carbon pool, indicating continuous replenishment of labile carbon pool from non-labile carbon pools within the hierarchy. The replenishment of labile carbon pool can be attributed mostly to decomposition of SOM1 and SOM2 pools with relatively faster turnover (Koven et al., 2013). Overall, we estimated the fast-decomposed carbon pool is approximately 2-4% of total SOC, similar 35 to previous estimates. The turnover time calculated from the fermentation rate was comparable to estimates of the turnover time of the fastest-responding carbon pool in previous studies (Figure 9), suggesting these quantifications and parameterization in the anaerobic carbon decomposition framework apply broadly.

4.4 Key features of the anaerobic model framework and future considerations

Here we present an anaerobic carbon decomposition framework by combining three well-known modeling approaches developed

Deleted: ,

Deleted: (Jones et al., 2003)

Deleted: be heterogeneous

Deleted: residual acidity or

Deleted: (Schädel et al., 2013).

Deleted: (Knoblauch et al., 2013).

Deleted: (Schädel et al., 2014)

Deleted: consistent

Deleted: (Phornton & Rosenbloom, 2005)

Deleted: 12

in different disciplines. A pool-based model to represent upstream carbon transformations and replenishment of DOC pool, a thermodynamically-based model to calculate rate kinetics and biomass growth for methanogenesis and Fe(III) reduction, and a humic ion-binding model for aqueous phase speciation and pH calculation are implemented into the open source geochemical model PHREEQC (Charlton & Parkhurst, 2011). The model framework presented here has several unique features. First, this model is built upon a thermodynamically-based approach, which allows consistent parameterization of individual reactions along the redox ladder. Such a model structure is particularly useful in circumstances when function-specific microbial growth is difficult to quantify and parameterize. Second, calculations of free energy changes of redox couples are used to modulate redox reaction hierarchy. Considering the difficulty in obtaining growth-associated parameters for every functional group, a thermodynamically-based approach significantly decreases the number of parameters that are difficult to measure. In addition, proton production and consumption during redox reactions are incorporated into a dynamic pH calculation, allowing various simulations on aqueous solubility and reactivity of different elements. The anaerobic carbon decomposition framework presented here holds a significant advantage over traditional models in simulating carbon decomposition process within a wide range of environmental settings.

In permafrost affected regions, studies consistently identify iron reduction, denitrification and sulfate reduction (Lipson et al., 2010; Lipson et al., 2013; Ernakovich et al., 2017; Hansen et al., 2007) as alternative anaerobic pathways, which are recognized as energetically more favorable processes than methanogenesis. The new model framework presented here provide a reasonable basis for a deeper understanding of carbon decomposition under oxygen-limited conditions where the importance of accounting for alternative electron acceptors becomes more pronounced. Future fine-scale experiments on carbon decomposition using alternative electron acceptors would be beneficial for more comprehensive parameterization of this model framework. Additional observations on temperature and pH sensitivity of specific redox reactions would also be quite useful in reducing large uncertainties generated by the current representation of temperature and pH responses. Application of such modeling framework at field scale requires close coupling with hydrology models to facilitate estimations on aqueous phase concentrations. Additional assumptions on vertical mixing and gas diffusion in the soil column should also be considered.

25 5. Conclusion

Microbial processes are the driving forces for biogeochemical cycling of soil carbon and are subjected to environmental constraints beyond temperature and organic substrate availability. The present study incorporated microbial redox reactions and mechanistic pH evolution to simulate anaerobic carbon decomposition in Arctic soils with depth and across soil moisture gradients. Our data synthesis and modeling results quantify direct effects of temperature on anaerobic carbon decomposition, as well as indirect effects of soil geochemistry that cause strong redox reaction-pH feedback. We identified substantial pH feedbacks on the predictions on CO₂ and CH₄ production. The anaerobic carbon decomposition framework presented in this study provided the essential model structure to incorporate redox reactions of alternative electron acceptors for accurate simulation of CO₂ and CH₄ production. Soil geochemistry impose critical constraints on SOM decomposition, and further regulates permafrost carbon feedback in response to changing climate.

35 Code and data availability

PHREEQC (Version 3) is publicly available at http://wwwbrr.cr.usgs.gov/projects/GWC_coupled/phreeqc/

Deleted: Fe(III)

Deleted: ,

Deleted: http://wwwbrr.cr.usgs.gov/projects/GWC_coupled/phreeqc/

Formatted: Underline

The model is archived at <https://dx.doi.org/10.5440/1430703>, with detailed description of model implementation, input files and various sensitivity analysis described in this paper.

5 Data sets used in this work can be found at

<https://dx.doi.org/10.5440/1168992>
<https://dx.doi.org/10.5440/1393836>
<https://dx.doi.org/10.5440/1288688>

Deleted: Input files for model simulation and sensitivity analysis can be found at
<https://github.com/jianqiz/decomposition>

Formatted: Font: No underline, (Intl) Arial Unicode MS

A synthesis of the the incubation data is available at

10 <https://doi.org/10.5440/1440029>

Author contributions

DG, SW, and BG conceived and organized the research study; PT, SP, DG and JZ built the conceptual model framework; JZ preformed all model simulations; JZ and DG drafted the manuscript. All authors contributed revisions to the manuscript and have given approval to the final version of the manuscript.

15

Competing interests

The authors declare no competing interests.

Acknowledgements

20 We appreciate comments and suggestions on earlier versions of this paper offered by Ethan Coon. The Next-Generation Ecosystem Experiments in the Arctic (NGEE Arctic) project is supported by the Biological and Environmental Research program in the U.S. Department of Energy (DOE) Office of Science. Oak Ridge National Laboratory is managed by UT-Battelle, LLC, for the DOE under Contract No. DE-AC05-00OR22725.

Deleted: <http://dx.doi.org/10.5440/1168992>
<http://dx.doi.org/10.5440/1393836>
<http://dx.doi.org/10.5440/1288688>

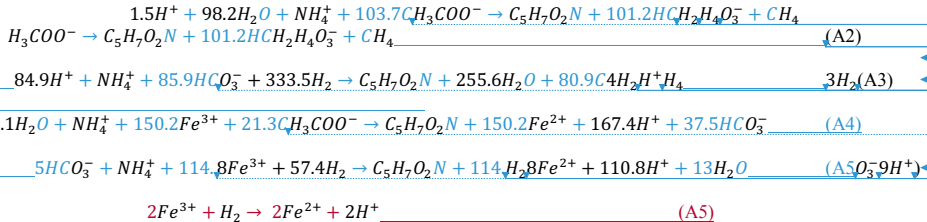
Appendix A: Anaerobic carbon decomposition model

25 This section lists reactions used in the anaerobic carbon decomposition model. Under anaerobic conditions, dissolved organic carbon is converted to low molecular weight organic acids via fermentation. One simplified fermentation reaction is used to represent this lumped fermentation process, where 1/3 of the fermented organic carbon is converted to CO₂ (Tang et al., 2016; Xu et al., 2015):



30 This fermentation reaction generates protons and decreases pH in the system. Fermentation products acetate and H₂ are further consumed via methanogenesis and iron reduction. The growth equations of methanogenesis and iron reduction were derived for each group using thermodynamically-based approach, in which biomass synthesis is included in paired electron donor and electron acceptor half-reactions. A general molecular formula C₅H₇O₂N is used for microbial biomass and the growth equations are written as (Istok et al., 2010).

Deleted: 1
Formatted: Left, Tab stops: 3.69", Centered + 6.5", Left
Deleted:
Deleted: (A2, A3)
Deleted: (A4, A5).
Deleted: implementation
Deleted: these reactions in PHREEQC was based on the bioenergetics of
Deleted: half reaction, electro
Deleted: reaction and cell synthesis to account
Formatted: Font color: Text 1
Formatted: Font color: Text 1
Formatted: Font color: Text 1
Deleted: of methanogens and iron reducers during the reactions.



In addition, Fe(III) was calculated based on the dissolution of representative amorphous ferric hydroxides (A6), which contributed to pH increase.

Appendix B: Temperature and pH response functions

We used the CLM_CN temperature response function (B1) in our simulations (Thornton and Rosenbloom, 2005). Additional tested temperature response functions included B2 used by CENTURY model (Parton et al., 2001), Arrhenius equation B3 used in ecosys (Grant, 1998), and the quadratic equation B4 (Ratkowsky et al., 1983). T_{ref} is set at 25 °C, E_a is the activation energy (J mol⁻¹), R is the universal gas constant (J K⁻¹ mol⁻¹). T_m used in Ratkowsky's model represents the conceptual temperature of no metabolic significant and is set at -8 °C in this study.

30
$$\ln f(T) = 308.56 \times \left(\frac{1}{71.02} - \frac{1}{T-227.13} \right) \quad (B1)$$

35
$$f(T) = 0.56 + 0.465 \arctan [0.097(T - 15.7)] \quad (B2)$$

40
$$f(T) = e^{\frac{-E_a}{R} \left(\frac{1}{T} - \frac{1}{T_{ref}} \right)} \quad (B3)$$

$$f(T) = \left(\frac{T-T_m}{T_{ref}-T_m} \right)^2$$

(B4)(T)
$$\left(\frac{T-T_m}{T_{ref}-T_m} \right)^2$$

45 The discontinuous bell-shaped pH response function from DLEM model was used here (equation B5, Tian et al., 2010)

$$f(pH) = \frac{1.02}{1.02 + 10^6 \exp(-2.5pH)} \quad (0 < pH < 7) \quad (B5)$$

50
$$f(pH) = \frac{1.02}{1.02 + 10^6 \exp(-2.5(14-pH))} - \frac{1.02}{1.02 + 10^6 \exp(-2.5(14-pH))} \quad (7 < pH < 14)$$

References

- Formatted: Left, Indent: Left: 0.5", Tab stops: 3.19", Centered + 6.5", Left
- Deleted: C
- Deleted: +H₂O → CH₄ + HC ... [16]
- Deleted: +H₂O → CH₄ + HC₂H₄O₃⁻ + CH₄ → ... [17]
- Formatted: Left, Tab stops: 3.56", Centered + 6.5", Left
- Formatted: Left, Tab stops: 3", Centered + 6.5", Left
- Deleted: HC₂H₄O₃⁻ + 333.5H₂O → C₅H₇O₂N + 255.6H₂O + 80.9C₄H₂H₄⁺ ... [18]
- Deleted: O
- Deleted: 1
- Formatted: Left, Tab stops: 3.31", Centered + 6.5", Left
- Deleted: +8Fe³⁺ + 57.4H₂O → C₅H₇O₂N + 114.4H₂O → 8Fe²⁺ + 110.8H⁺ + 13H₂O (A52HC) ... [19]
- Deleted: +9H⁺ (A4) ... [20]
- Deleted: 1
- Formatted: Left
- Deleted:
- Formatted: Left, Tab stops: 3.25", Centered + 6.5", Left
- Deleted: We used the CLM_CN temperature response function (B1) in our simulations (Thornton and Rosenbloom, 2005). Additional temperature response functions tested here including B2 used by CENTURY model (Parton et al., 2001), Arrhenius equation B3 used in ecosys (Grant, 1998), and the quadratic equation B4 (Ratkowsky et al., 1983). T_{ref} is set at 25 °C, E_a is the activation energy (J mol⁻¹), R is the universal gas constant (J K⁻¹ mol⁻¹). T_m used in Ratkowsky's model represents the conceptual temperature of no metabolic significant and is set at -8 °C in this study.
- Formatted ... [22]
- Deleted:
- Deleted:
- Formatted ... [23]
- Deleted: →
- Formatted ... [24]
- Deleted: f
- Deleted: $\left(\frac{T-T_m}{T_{ref}-T_m} \right)^2$... [25]
- Formatted ... [26]
- Deleted: ... 0 < pH < 7) → ... [27]
- Formatted ... [28]
- Deleted:
- Deleted: 1
- Deleted: Reference

Formatted: Level 1

Formatted: Font: Bold

Atalay, Y. B., Carbonaro, R. F., and Di Toro, D. M.: Distribution of Proton Dissociation Constants for Model Humic and Fulvic Acid Molecules, *Environmental Science & Technology*, 43, 3626-3631, 10.1021/es03057r, 2009.

Bethke, C. M., Sanford, R. A., Kirk, M. F., Jin, Q., and Flynn, T. M.: The thermodynamic ladder in geomicrobiology, *American Journal of Science*, 311, 183-210, 10.2475/03.2011.01, 2011.

Blumer-Schuette, S. E., Brown, S. D., Sander, K. B., Bayer, E. A., Kataeva, I., Zurawski, J. V., Conway, J. M., Adams, M. W., and Kelly, R. M.: Thermophilic lignocellulose deconstruction, *FEMS Microbiol. Rev.*, 38, 393-448, 10.1111/1574-6976.12044, 2014.

Charlton, S., and Parkhurst, D.: Modules based on the geochemical model PHREEQC for use in scripting and programming languages, *Computers & Geosciences*, 37(10), 1653-1663, <https://doi.org/10.1016/j.cageo.2011.02.005>, 2011.

Drake, T. W., Wickland, K. P., Spencer, R. G. M., McKnight, D. M., and Stiegl, R. G.: Ancient low-molecular-weight organic acids in permafrost fuel rapid carbon dioxide production upon thaw, *Proceedings of the National Academy of Sciences*, 112, 13946-13951, 10.1073/pnas.1511705112, 2015.

Dudal Y., Férid, F.: Accounting for natural organic matter in aqueous chemical equilibrium models: a review of the theories and applications, *Earth-Science Reviews*, 66, 199-216, <https://doi.org/10.1016/j.earscirev.2004.01.002>, 2004.

Elberling, B., Michelsen, A., Schadel, C., Schuur, E. A. G., Christiansen, H. H., Berg, L., Tamstorf, M. P., and Sigsgaard, C.: Long-term CO₂ production following permafrost thaw, *Nature Clim. Change*, 3, 890-894, 10.1038/nclimate1955, 2013.

Ernakovitch, J. G., Lynch, L. M., Brewer, P. E., Calderon, F. J., and Wallenstein, M. D.: Redox and temperature-sensitive changes in microbial communities and soil chemistry dictate greenhouse gas loss from thawed permafrost, *Biogeochemistry*, 134, 183-200, 10.1007/s10533-017-0354-5, 2017.

French, H. M.: *The Periglacial Environment*, 3rd ed., John Wiley & Sons, Chichester, 2007.

Glissmann, K., and Conrad, R.: Saccharolytic activity and its role as a limiting step in methane formation during the anaerobic degradation of rice straw in rice paddy soil, *Biology and Fertility of Soils*, 35, 62-67, 10.1007/s00374-002-0442-z, 2002.

Grant, R. F.: Simulation of methanogenesis in the mathematical model ecosys, *Soil Biology and Biochemistry*, 30, 883-896, [http://dx.doi.org/10.1016/S0038-0717\(97\)00218-6](http://dx.doi.org/10.1016/S0038-0717(97)00218-6), 1998.

Grant, R. F.: Simulation of methanotrophy in the mathematical model ecosys, *Soil Biology and Biochemistry*, 31, 287-297, [http://dx.doi.org/10.1016/S0038-0717\(98\)00119-9](http://dx.doi.org/10.1016/S0038-0717(98)00119-9), 1999.

Hansen, A. A., Herbert, R. A., Mikkelsen, K., Jensen, L. L., Kristoffersen, T., Tiedje, J. M., Lomstein, B. A., and Finster, K. W.: Viability, diversity and composition of the bacterial community in a high Arctic permafrost soil from Spitsbergen, Northern Norway, *Environmental Microbiology*, 9, 2870-2884, 10.1111/j.1462-2920.2007.01403.x, 2007.

Herndon, E. M., Mann, B. F., Roy Chowdhury, T., Yang, Z., Wullschleger, S. D., Graham, D., Liang, L., and Gu, B.: Pathways of anaerobic organic matter decomposition in tundra soils from Barrow, Alaska, *Journal of Geophysical Research: Biogeosciences*, 120, 2345-2359, 10.1002/2015JG003147, 2015.

Herndon, E. M., Yang, Z., and B., G.: Soil Organic Carbon Degradation during Incubation, Barrow, Alaska, 2012. Next Generation Ecosystem Experiments Arctic Data Collection, Carbon Dioxide Information Analysis Center, Oak Ridge National Laboratory, Oak Ridge, Tennessee, USA. Data set accessed at <http://dx.doi.org/10.5440/1168992> 2016.

Høj, L., Rusten, M., Haugen, L. E., Olsen, R. A., and Torsvik, V. L.: Effects of water regime on archaeal community composition in Arctic soils, *Environmental Microbiology*, 8, 984-996, 10.1111/j.1462-2920.2006.00982.x, 2006.

Howell, J., Donahoe, R., Roden, E., and Ferris, F.: Effects of microbial iron oxide reduction on pH and alkalinity in anaerobic bicarbonate-buffered media: implications for metal mobility, *Mineralogical Magazine*, 62A:657-658, 1998.

Hunter, J. D.: Matplotlib: A 2D Graphics Environment, *Computing in Science & Engineering*, 9, 90-95, 10.1109/MCSE.2007.55, 2007.

Istok, J. D., Park, M., Michalsen, M., Spain, A. M., Krumholz, L. R., Liu, C., McKinley, J., Long, P., Roden, E., Peacock, A. D., and Baldwin, B.: A thermodynamically-based model for predicting microbial growth and community composition coupled to system geochemistry: Application to uranium bioreduction, *Journal of Contaminant Hydrology*, 112, 1-14, <https://doi.org/10.1016/j.jconhyd.2009.07.004>, 2010.

Jones, D. L., Dennis, P. G., Owen, A. G., and van Hees, P. A. W.: Organic acid behavior in soils – misconceptions and knowledge gaps, *Plant and Soil*, 248, 31-41, 10.1023/a:1022304332313, 2003.

Karhu, K., Aufret, M. D., Dungait, J. A. J., Hopkins, D. W., Prosser, J. I., Singh, B. K., Subke, J.-A., Wookey, P. A., Agren, G. I., Sebastian, M.-T., Gouriveau, F., Bergkvist, G., Meir, P., Nottingham, A. T., Salinas, N., and Hartley, I. P.: Temperature sensitivity of soil respiration rates enhanced by microbial community response, *Nature*, 513, 81-84, 10.1038/nature13604, 2014.

Knoblauch, C., Beer, C., Sosnin, A., Wagner, D., and Pfeiffer, E.-M.: Predicting long-term carbon mineralization and trace gas production from thawing permafrost of Northeast Siberia, *Global Change Biology*, 19, 1160-1172, 10.1111/gcb.12116, 2013.

Kotsyurbenko, O. R.: Trophic interactions in the methanogenic microbial community of low-temperature terrestrial ecosystems, *FEMS Microbiology Ecology*, 53, 3-13, <http://dx.doi.org/10.1016/j.femsec.2004.12.009>, 2005.

Koven, C. D., Lawrence, D. M., and Riley, W. J.: Permafrost carbon–climate feedback is sensitive to deep soil carbon decomposability but not deep soil nitrogen dynamics, *Proceedings of the National Academy of Sciences*, 112, 3752-3757, 10.1073/pnas.1415123112, 2015.

Koven, C. D., Hugelius, G., Lawrence, D. M., and Wieder, W. R.: Higher climatological temperature sensitivity of soil carbon in cold than warm climates, *Nature Clim. Change*, 7, 817, 10.1038/nclimate3421, 2017.

Lawrence, D. M., Koven, C. D., Swenson, S. C., Riley, W. J., and Slater, A. G.: Permafrost thaw and resulting soil moisture changes regulate projected high-latitude CO₂ and CH₄ emissions, *Environmental Research Letters*, 10, 094011, 2015.

5 Lee, H., Schuur, E. A. G., Inglett, K. S., Lavoie, M., and Chanton, J. P.: The rate of permafrost carbon release under aerobic and anaerobic conditions and its potential effects on climate, *Global Change Biology*, 18, 515-527, 10.1111/j.1365-2486.2011.02519.x, 2012.

Liljedahl, A. K., Boike, J., Daanen, R. P., Fedorov, A. N., Frost, G. V., Grossé, G., Hinzman, L. D., Iijima, Y., Jorgenson, J. C., Matveyeva, N., Necsoiu, M., Reynolds, M. K., Romanovsky, V. E., Schulla, J., Tape, K. D., Walker, D. A., Wilson, C. J., 10 Yabuki, H., and Zona, D.: Pan-Arctic ice-wedge degradation in warming permafrost and its influence on tundra hydrology, *Nature Geosci.*, 9, 312-318, 10.1038/ngeo2674, 2016.

Lipson, D. A., Jha, M., Raab, T. K., and Oechel, W. C.: Reduction of iron (III) and humic substances plays a major role in anaerobic respiration in an Arctic peat soil, *J. Geophys. Res.*, 115, G00106, 10.1029/2009jg001147, 2010.

Lipson, D. A., Raab, T. K., Goria, D., and Zlamal, J.: The contribution of Fe(III) and humic acid reduction to ecosystem 15 respiration in drained thaw lake basins of the Arctic Coastal Plain, *Global Biogeochemical Cycles*, 27, 399-409, 10.1002/gbc.20038, 2013.

Lupascu, M., Wadham, J. L., Hornbrook, E. R. C., and Pancost, R. D.: Temperature Sensitivity of Methane Production in the Permafrost Active Layer at Stordalen, Sweden: A Comparison with Non-permafrost Northern Wetlands, Arctic, Antarctic, and Alpine Research, 44, 469-482, 10.1657/1938-4246-44.4.469, 2012.

20 MacDougall, A. H., Avis, C. A., and Weaver, A. J.: Significant contribution to climate warming from the permafrost carbon feedback, *Nature Geosci.*, 5, 719-721, 2012.

Manzoni, S., and Porporato, A.: Soil carbon and nitrogen mineralization: Theory and models across scales, *Soil Biology and Biochemistry*, 41, 1355-1379, <http://dx.doi.org/10.1016/j.soilbio.2009.02.031>, 2009.

25 McGuire, A. D., Christensen, T. R., Hayes, D., Heroult, A., Euskirchen, E., Kimball, J. S., Koven, C., Lafleur, P., Miller, P. A., Oechel, W., Peylin, P., Williams, M., and Yi, Y.: An assessment of the carbon balance of Arctic tundra: comparisons among observations, process models, and atmospheric inversions, *Biogeosciences*, 9, 3185-3204, 10.5194/bg-9-3185-2012, 2012.

Meng, L., Hess, P. G. M., Mahowald, N. M., Yavitt, J. B., Riley, W. J., Subin, Z. M., Lawrence, D. M., Swenson, S. C., Jauhainen, J., and Fuka, D. R.: Sensitivity of wetland methane emissions to model assumptions: application and model testing against site observations, *Biogeosciences*, 9, 2793-2819, 10.5194/bg-9-2793-2012, 2012.

30 Newman, B. D., Throckmorton, H. M., Graham, D. E., Gu, B., Hubbard, S. S., Liang, L., Wu, Y., Heikoop, J. M., Herndon, E. M., Phelps, T. J., Wilson, C. J., and Wullschleger, S. D.: Microtopographic and depth controls on active layer chemistry in Arctic polygonal ground, *Geophys. Res. Lett.*, 42, 1808-1817, 10.1002/2014GL062804, 2015.

Oliphant, T. E.: Python for Scientific Computing, *Computing in Science & Engineering*, 9, 10-20, 10.1109/MCSE.2007.58, 2007.

35 Painter, S. L., Moulton, J. D., and Wilson, C. J.: Modeling challenges for predicting hydrologic response to degrading permafrost, *Hydrogeology Journal*, 21, 221-224, 10.1007/s10040-012-0917-4, 2013.

Parton, B., Ojima, D., Del Grosso, S., Keough, C.: CENTURY Tutorial. Supplement to CENTURY User's Manual. NREC Pub. Natural Resource Ecology Laboratory, Colorado State University; Fort Collins, CO, USA. Great Plain System. Research Unit Technical Report No. 4, 2001.

40 Ratkowsky, D. A., Olley, J., McMeekin, T. A., and Ball, A.: Relationship between temperature and growth rate of bacterial cultures, *J. Bacteriol.*, 149, 1-5, 1982.

Ratkowsky, D. A., Lowry, R. K., McMeekin, T. A., Stokes, A. N., and Chandler, R. E.: Model for bacterial culture growth rate throughout the entire biokinetic temperature range, *Journal of Bacteriology*, 154, 1222-1226, 1983.

Riley, W. J., Subin, Z. M., Lawrence, D. M., Swenson, S. C., Torn, M. S., Meng, L., Mahowald, N. M., and Hess, P.: Barriers to 45 predicting changes in global terrestrial methane fluxes: analyses using CLM4Me, a methane biogeochemistry model integrated in CESM, *Biogeosciences*, 8, 1925-1953, 10.5194/bg-8-1925-2011, 2011.

Rivkina, E., Shcherbakova, V., Laurinavicius, K., Petrovskaya, L., Krivushin, K., Kraev, G., Pecheritsina, S., and Gilichinsky, D.: Biogeochemistry of methane and methanogenic archaea in permafrost, *FEMS Microbiology Ecology*, 61, 1-15, 10.1111/j.1574-6941.2007.00315.x, 2007.

50 Roy Chowdhury, T., Herndon, E. M., Phelps, T. J., Elias, D. A., Gu, B., Liang, L., Wullschleger, S. D., and Graham, D. E.: Stoichiometry and temperature sensitivity of methanogenesis and CO₂ production from saturated polygonal tundra in Barrow, Alaska, *Global Change Biology*, 21, 722-737, 10.1111/gcb.12762, 2015.

Sarkar, D.: Lattice: Multivariate Data Visualization with R. Springer, New York. ISBN 978-0-387-75968-5, 2008.

Schädel, C., Bader, M. K. F., Schuur, E. A. G., Biasi, C., Bracho, R., Capek, P., De Baets, S., Diakova, K., Ernakovich, J., Estop-55 Aragones, C., Graham, D. E., Hartley, I. P., Iversen, C. M., Kane, E., Knoblauch, C., Lupascu, M., Martikainen, P. J., Natali, S. M., Norby, R. J., O'Donnell, J. A., Chowdhury, T. R., Santrukova, H., Shaver, G., Sloan, V. L., Treat, C. C., Turetsky, M. R., Waldrop, M. P., and Wickland, K. P.: Potential carbon emissions dominated by carbon dioxide from thawed permafrost soils, *Nature Clim. Change*, 6, 950-953, 10.1038/nclimate3054, 2016.

Schädel, C., Luo, Y., David Evans, R., Fei, S., and Schaeffer, S. M.: Separating soil CO₂ efflux into C-pool-specific decay rates via inverse analysis of soil incubation data, *Oecologia*, 171, 721-732, 10.1007/s00442-012-2577-4, 2013.

Schädel, C., Schuur, E. A. G., Bracho, R., Elberling, B., Knoblauch, C., Lee, H., Luo, Y., Shaver, G. R., and Turetsky, M. R.: Circumpolar assessment of permafrost C quality and its vulnerability over time using long-term incubation data, *Global Change Biology*, 20, 641-652, 10.1111/geb.12417, 2014.

Schaefer, K., Hugues, L., Vladimir, E. R., Edward, A. G. S., and Ronald, W.: The impact of the permafrost carbon feedback on global climate, *Environmental Research Letters*, 9, 085003, 2014.

Schuur, E. A. G., Vogel, J. G., Crummer, K. G., Lee, H., Sickman, J. O., and Osterkamp, T. E.: The effect of permafrost thaw on old carbon release and net carbon exchange from tundra, *Nature*, 459, 556-559, 2009.

Schuur, E. A. G., McGuire, A. D., Schädel, C., Grosse, G., Harden, J. W., Hayes, D. J., Hugelius, G., Koven, C. D., Kuhr, P., Lawrence, D. M., Natali, S. M., Olefeldt, D., Romanovsky, V. E., Schaefer, K., Turetsky, M. R., Treat, C. C., and Vonk, J. E.: Climate change and the permafrost carbon feedback, *Nature*, 520, 171-179, 10.1038/nature14338, 2015.

Segers, R.: Methane production and methane consumption: a review of processes underlying wetland methane fluxes, *Biogeochemistry*, 41, 23-51, 10.1023/a:1005929032764, 1998.

Segers, R., and Leffelaar, P. A.: Modeling methane fluxes in wetlands with gas-transporting plants: 3. Plot scale, *Journal of Geophysical Research: Atmospheres*, 106, 3541-3558, 10.1029/2000JD900482, 2001a.

Segers, R., and Leffelaar, P. A.: Modeling methane fluxes in wetlands with gas-transporting plants: 1. Single-root scale, *Journal of Geophysical Research: Atmospheres*, 106, 3511-3528, 10.1029/2000JD900484, 2001b.

Segers, R., Rappoldt, C., and Leffelaar, P. A.: Modeling methane fluxes in wetlands with gas-transporting plants: 2. Soil layer scale, *Journal of Geophysical Research: Atmospheres*, 106, 3529-3540, 10.1029/2000JD900483, 2001.

Tang, G., Zheng, J., Xu, X., Yang, Z., Graham, D. E., Gu, B., Painter, S. L., and Thornton, P. E.: Biogeochemical modeling of CO_2 and CH_4 production in anoxic Arctic soil microcosms, *Biogeosciences*, 13, 5021-5041, 10.5194/bg-13-5021-2016, 2016.

Tarnocai, C., Canadell, J. G., Schuur, E. A. G., Kuhr, P., Mazhitova, G., and Zimov, S.: Soil organic carbon pools in the northern circumpolar permafrost region, *Global Biogeochemical Cycles*, 23, GB2023, 10.1029/2008GB003327, 2009.

Thornton, P. E., and Rosenbloom, N. A.: Ecosystem model spin-up: Estimating steady state conditions in a coupled terrestrial carbon and nitrogen cycle model, *Ecological Modelling*, 189, 25-48, <https://doi.org/10.1016/j.ecolmodel.2005.04.008>, 2005.

Tian, H., Xu, X., Liu, M., Ren, W., Zhang, C., Chen, G., and Lu, C.: Spatial and temporal patterns of CH_4 and N_2O fluxes in terrestrial ecosystems of North America during 1979-2008: application of a global biogeochemistry model, *Biogeosciences*, 7, 2673-2694, <https://doi.org/10.5194/bg-7-2673-2010>, 2010.

Tilston, E. L., Sparreman, T., and Öquist, M. G.: Unfrozen water content moderates temperature dependence of sub-zero microbial respiration, *Soil Biology and Biochemistry*, 42, 1396-1407, <https://doi.org/10.1016/j.soilbio.2010.04.018>, 2010.

Tipping, E.: WHAM: a chemical equilibrium model and computer code for waters, sediments, and soils incorporating a discrete site/electrostatic model of ion-binding by humic substances, *Comput. Geosci.*, 20, 973-1023, 10.1016/0098-3004(94)90038-8, 1994.

Tipping, E.: Humic Ion-Binding Model VI: An Improved Description of the Interactions of Protons and Metal Ions with Humic Substances, *Aquatic Geochemistry*, 4, 3-47, 10.1023/a:1009627214459, 1998.

Treat, C. C., Wollheim, W. M., Varner, R. K., Grandy, A. S., Talbot, J., and Frolking, S.: Temperature and peat type control CO_2 and CH_4 production in Alaskan permafrost peats, *Global Change Biology*, 20, 2674-2686, 10.1111/gcb.12572, 2014.

Treat, C. C., Natali, S. M., Ernakovitch, J., Iversen, C. M., Lupascu, M., McGuire, A. D., Norby, R. J., Roy Chowdhury, T., Richter, A., Šantrúčková, H., Schädel, C., Schuur, E. A. G., Sloan, V. L., Turetsky, M. R., and Waldrop, M. P.: A pan-Arctic synthesis of CH_4 and CO_2 production from anoxic soil incubations, *Global Change Biology*, 21, 2787-2803, 10.1111/gcb.12875, 2015.

Tuomi, M., Vanhala, P., Karhu, K., Fritze, H., and Liski, J.: Heterotrophic soil respiration—Comparison of different models describing its temperature dependence, *Ecol. Model.*, 211, 182-190, <https://doi.org/10.1016/j.ecolmodel.2007.09.003>, 2008.

Vaughn, L. J. S., Conrad, M. E., Bill, M., and Torn, M. S.: Isotopic insights into methane production, oxidation, and emissions in Arctic polygon tundra, *Glob. Change Biol.*, 22, 3487-3502, 10.1111/gcb.13281, 2016.

Venables, W. N., and Ripley, B. D.: MASS: Modern Applied Statistics with S. Fourth Edition. Springer, New York. ISBN 0-387-95457-0, 2002.

Wachinger, G., Fiedler, S., Zepp, K., Gattinger, A., Sommer, M., and Roth, K.: Variability of soil methane production on the micro-scale: spatial association with hot spots of organic material and Archaeal populations, *Soil Biology and Biochemistry*, 32, 1121-1130, [https://doi.org/10.1016/S0038-0717\(00\)00024-9](https://doi.org/10.1016/S0038-0717(00)00024-9), 2000.

Wagner, R., Zona, D., Oechel, W., and Lipson, D.: Microbial community structure and soil pH correspond to methane production in Arctic Alaska soils, *Environ. Microbiol.*, 19, 3398-3410, 10.1111/1462-2920.13854, 2017.

Waldrop, M. P., Wickland, K. P., White III, R., Berhe, A. A., Harden, J. W., and Romanovsky, V. E.: Molecular investigations into globally important carbon pool: permafrost-protected carbon in Alaskan soils, *Global Change Biology*, 16, 2543-2554, 10.1111/j.1365-2486.2009.02141.x, 2010.

Walt, S. v. d., Colbert, S. C., and Varoquaux, G.: The NumPy Array: A Structure for Efficient Numerical Computation, *Computing in Science & Engineering*, 13, 22-30, 10.1109/mcse.2011.37, 2011.

Walz J., Knoblauch C., Böhme L., Pfeiffer E.M.: Regulation of soil organic matter decomposition in permafrost-affected Siberian tundra soils - Impact of oxygen availability, freezing and thawing, temperature, and labile organic matter. *Soil Biology and Biochemistry* **110**: 34-43.2017.

Walvoord, M. A., and Kurylyk, B. L.: Hydrologic Impacts of Thawing Permafrost—A Review, *Vadose Zone Journal*, 15, 10.2136/vzj2016.01.0010, 2016.

Wickham, H.: *ggplot2: Elegant Graphics for Data Analysis*. Springer-Verlag New York, 2009, 2009.

Wickham, H., Francois, R., Henry, L., and Müller, K.: *dplyr: A Grammar of Data Manipulation*. R package version 0.7.3. <https://CRAN.R-project.org/package=dplyr>, 2017.

Xu, X., Elias, D. A., Graham, D. E., Phelps, T. J., Carroll, S. L., Wullschleger, S. D., and Thornton, P. E.: A microbial functional group-based module for simulating methane production and consumption: Application to an incubated permafrost soil, *Journal of Geophysical Research: Biogeosciences*, 120, 1315-1333, 10.1002/2015JG002935, 2015.

Xu, X., Yuan, F., Hanson, P. J., Wullschleger, S. D., Thornton, P. E., Riley, W. J., Song, X., Graham, D. E., Song, C., and Tian, H.: Reviews and syntheses: Four decades of modeling methane cycling in terrestrial ecosystems, *Biogeosciences*, 13, 3735-3755, 10.5194/bg-13-3735-2016, 2016.

Yang, S., Liebner, S., Winkel, M., Alawi, M., Horn, F., Dörfer, C., Ollivier, J., He, J.-s., Jin, H., Kühn, P., Schloter, M., Scholten, T., and Wagner, D.: In-depth analysis of core methanogenic communities from high elevation permafrost-affected wetlands, *Soil Biology and Biochemistry*, 111, 66-77, <https://doi.org/10.1016/j.soilbio.2017.03.007>, 2017.

Yang, Z., Wullschleger, S. D., Liang, L., Graham, D. E., and Gu, B.: Effects of warming on the degradation and production of low-molecular-weight labile organic carbon in an Arctic tundra soil, *Soil Biol. Biochem.*, 95, 202-211, <http://dx.doi.org/10.1016/j.soilbio.2015.12.022>, 2016.

Yvon-Durocher, G., Caffrey, J. M., Cescatti, A., Dossena, M., Giorgio, P. d., Gasol, J. M., Montoya, J. M., Pumpanen, J., Staehr, P. A., Trimmer, M., Woodward, G., and Allen, A. P.: Reconciling the temperature dependence of respiration across timescales and ecosystem types, *Nature*, 487, 472-476, <http://www.nature.com/nature/journal/v487/n7408/abs/nature11205.html#supplementary-information>, 2012.

Yvon-Durocher, G., Allen, A. P., Bastviken, D., Conrad, R., Gudasz, C., St-Pierre, A., Thanh-Duc, N., and del Giorgio, P. A.: Methane fluxes show consistent temperature dependence across microbial to ecosystem scales, *Nature*, 507, 488-491, 10.1038/nature13164, 2014.

Zheng, J., Roy Chowdhury, T., and Graham, D.: CO₂ and CH₄ Production and CH₄ Oxidation in Low Temperature Soil Incubations from Flat- and High-Centered Polygons, Barrow, Alaska, 2012. Next Generation Ecosystem Experiments Arctic Data Collection, Oak Ridge National Laboratory, U.S. Department of Energy, Oak Ridge, Tennessee, USA. Dataset accessed at <http://dx.doi.org/10.5440/1288688>, 2016.

Zheng, J., and Graham, D.: Soil Organic Carbon Degradation in Low Temperature Soil Incubations from Flat- and High-Centered Polygons, Barrow, Alaska, 2012-2013. Next Generation Ecosystem Experiments Arctic Data Collection, Oak Ridge National Laboratory, U.S. Department of Energy, Oak Ridge, Tennessee, USA. Dataset accessed at <http://dx.doi.org/10.5440/1393836>, 2017.

Zheng, J., Roy Chowdhury, T., Yang, Z., Gu, B., Wullschleger, S., Graham, D., : Impacts of temperature and soil characteristics on methane production and oxidation in Arctic polygon tundra, *Biogeosciences Discuss.*, <https://doi.org/10.5194/bg-2017-566>, in review, 2018.

Zhuang, Q., Melillo, J. M., Sarofim, M. C., Kicklighter, D. W., McGuire, A. D., Felzer, B. S., Sokolov, A., Prinn, R. G., Steudler, P. A., and Hu, S.: CO₂ and CH₄ exchanges between land ecosystems and the atmosphere in northern high latitudes over the 21st century, *Geophysical Research Letters*, 33, n/a-n/a, 10.1029/2006GL026972, 2006.

Zimov, S. A., Schuur, E. A. G., and Chapin, F. S.: Permafrost and the Global Carbon Budget, *Science*, 312, 1612-1613, 10.1126/science.1128908, 2006.

Formatted: Font: Font color: Black, Border: : (No border), Pattern: Clear

Formatted: Authors, Indent: Left: -0.5", Hanging: 0.5", No widow/orphan control, Don't swap indents on facing pages, Tab stops: 0.39", Left + 0.78", Left + 1.17", Left + 1.56", Left + 1.94", Left + 2.33", Left + 2.72", Left + 3.11", Left + 3.5", Left + 3.89", Left + 4.28", Left + 4.67", Left

Deleted: [1](#)

Formatted: Indent: Hanging: 0.5", Don't swap indents on facing pages

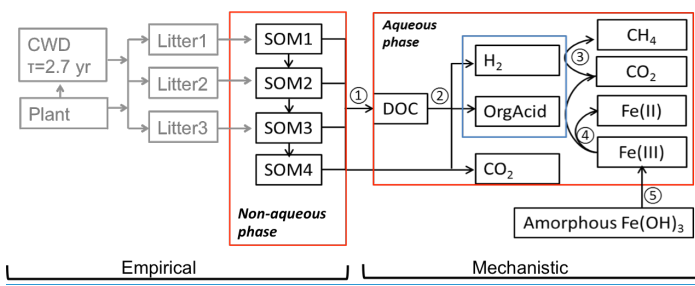
Deleted: [1](#)

Table 1. Descriptive statistics and correlation matrix for soil geochemical characteristics, labile carbon pool (in $\mu\text{mol g}^{-1}$ C) and estimated 60 days max production of CO₂ and CH₄ (in $\mu\text{mol g}^{-1}$ C) at 8 and -2°C [1](#)

... [29]

Formatted: Indent: Hanging: 0.5", Line spacing: single, Don't swap indents on facing pages

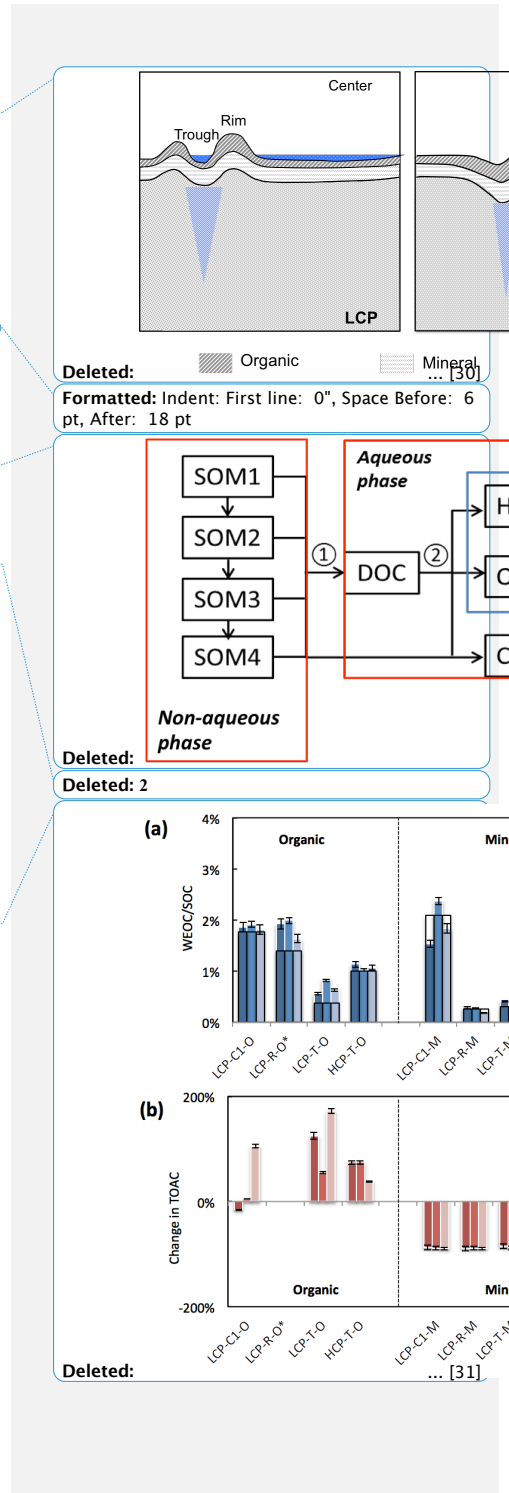
Formatted: Font: Bold, (Intl) Arial Unicode MS



5
Figure 1. Conceptual diagram showing key processes in the anaerobic carbon decomposition framework. The numbers indicate different processes: 1. SOM degradation from soil organic carbon pools with increasing turnover time produces dissolved organic carbon (DOC) and CO_2 ; 2. Fermentation of DOC into organic acids, H_2 and CO_2 ; 3. Methanogenesis from organic acids or H_2 ; 4. Fe(III) reduction from organic acids or H_2 ; 5. Fe(OH)_3 dissolution.

10

15



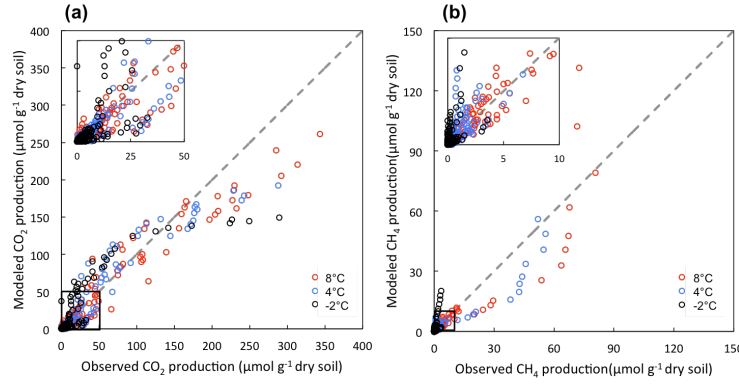
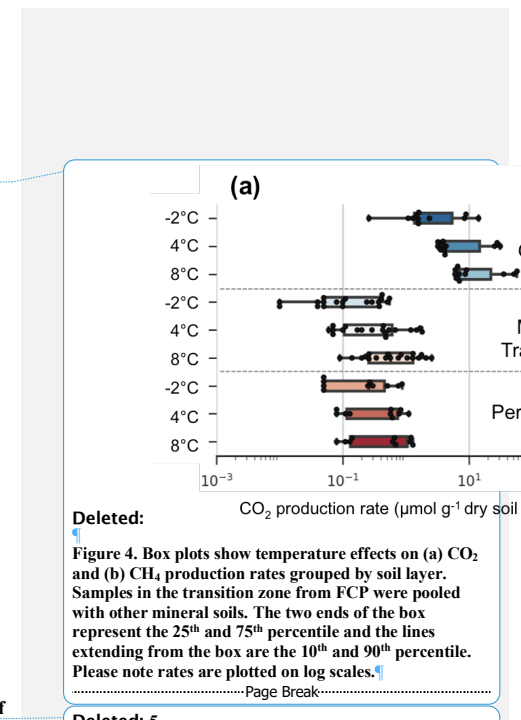


Figure 2. Comparison between modeled and observed production of CO₂ (a) and CH₄ (b). Averaged measurements of triplicate microcosms at each time point from each incubation temperature were calculated as observed values.



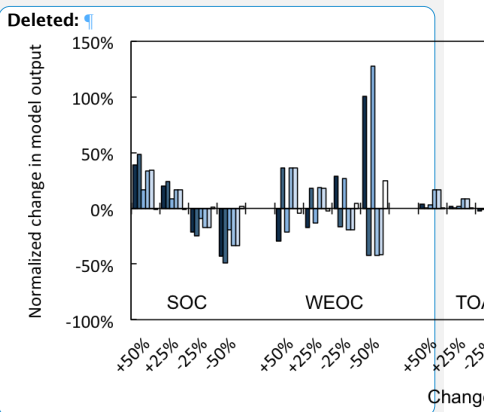
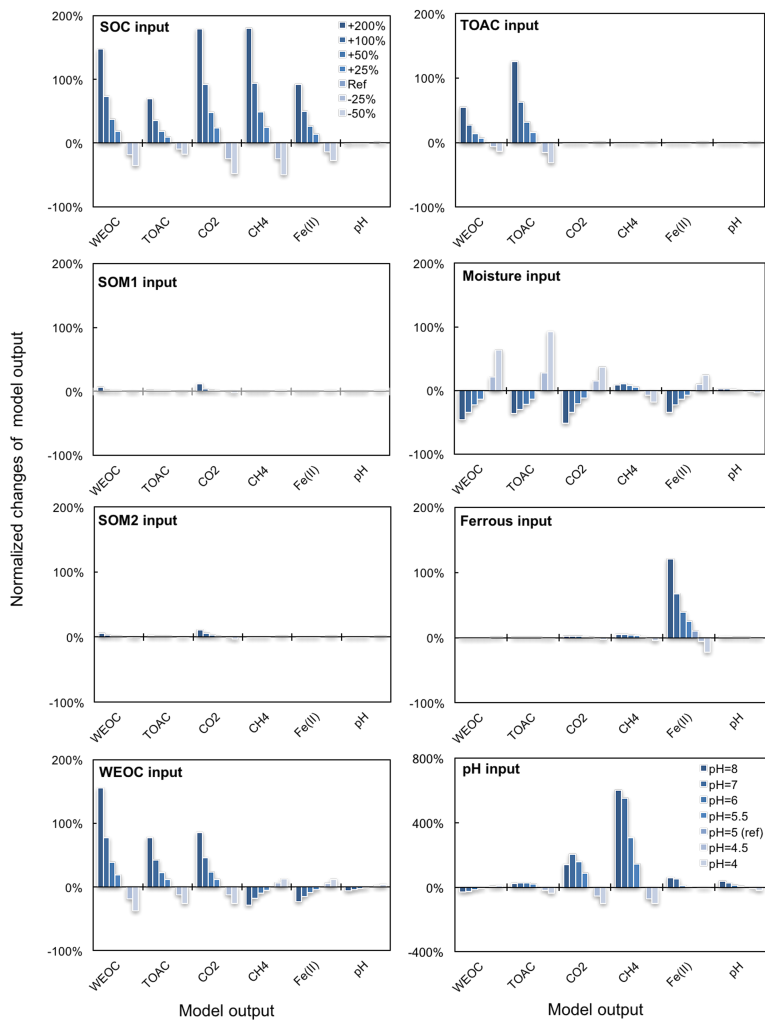


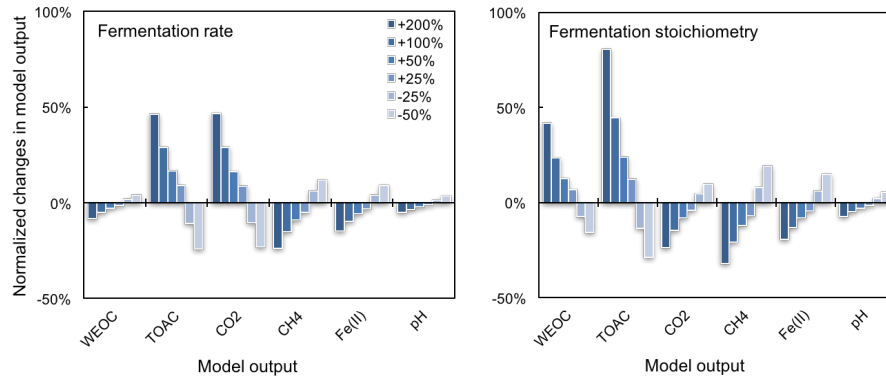
Figure 3. Perturbations of initial soil geochemical conditions differentially affected model predictions (including CH₄, CO₂,

5 Fe(II), TOAC, WEOC, and pH) during anaerobic carbon decomposition. [For example, when the initial pH decreased by 8% and 17%, CH₄ production decreased by 40% and 80%, respectively.](#) Normalized changes in model output were calculated as the ratio of perturbation simulation output to reference simulation output after 60 days of anaerobic decomposition at 8 °C. To test model sensitivity in response to initial pH, the reference run started with pH 6, and up to 1 pH unit changes was applied in perturbation simulations to represent a realistic pH range for soils. Reference simulations

Deleted: 6

were based on soils with 30% SOC (water content=2 g g⁻¹ dwt, and pH=5).

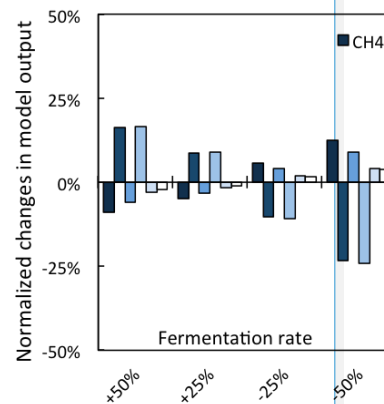
Deleted:Page Break.....



5

Figure 4. Simulated changes in model predictions (including CH₄, CO₂, Fe(II), TOAC, WEOC, and pH) during anaerobic carbon decomposition in response to perturbations of (a) fermentation rate and (b) fermentation stoichiometry (Acetate:CO₂=1:1 for reference simulation). Normalized changes in model output were calculated as the ratio of perturbation simulation output to reference simulation output after 60 days of anaerobic decomposition at 8 °C. Reference simulations were based on soils with 30% SOC (water content=2 g g⁻¹ dwt, and pH=5).

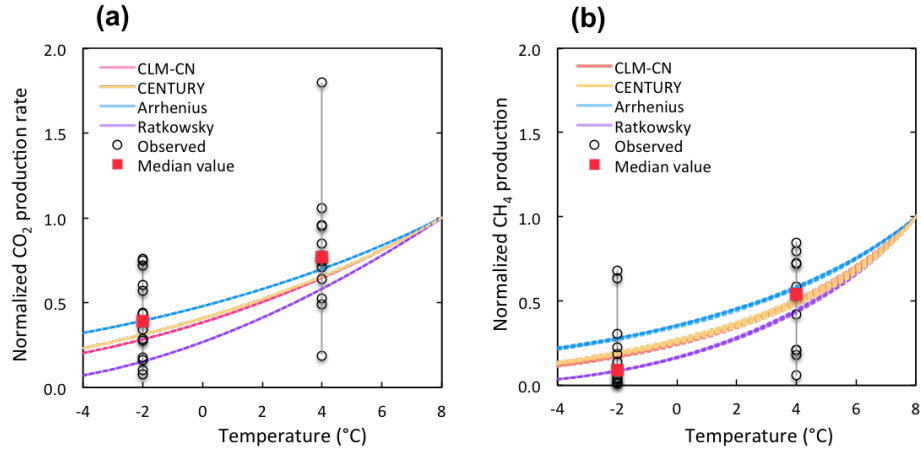
10



Deleted:

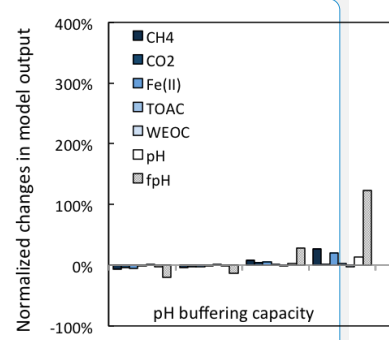
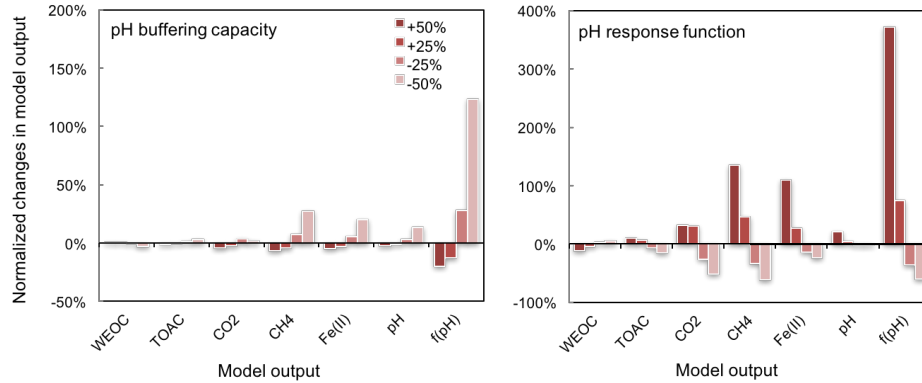
Deleted: 7

Deleted: SOM1, SOM2



5 **Figure 5. Comparison of simulated and observed temperature response for the production of CO₂ (a) and CH₄ (b).** Results were all normalized to CO₂ or CH₄ production rates at 8 °C for direct comparison. Observations at -2°C and 4 °C were plotted in black dots and the median value were marked in red. The shaded area represents output uncertainties generated from rate estimations within 60±5 days. Reference simulations were based on soils with 30% SOC (water content=2 g g⁻¹ dwt, and pH=5).

Deleted: 8



Deleted:

Deleted: 9

5 **Figure 6. Simulated changes in model predictions (including CH₄, CO₂, Fe(II), TOAC, WEOC, pH and *f_{pH}*) during anaerobic carbon decomposition in response to perturbations of (a) pH buffering capacity, and (b) pH response function. Normalized changes in model output were calculated as the ratio of perturbation simulation output to reference simulation output after 60 days of anaerobic decomposition at 8 °C. Reference simulations were based on soils with 30% SOC (water content=2 g g⁻¹ dwt, and pH=5).**

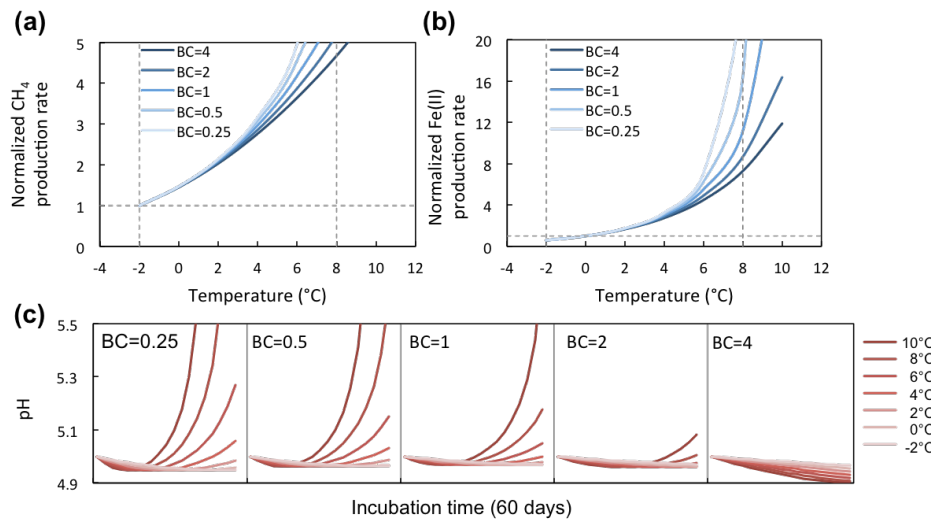


Figure 7. Temperature response of CH_4 and Fe(II) production rates at varying soil pH buffering capacities (BC). Varying BCs with respect to reference simulation (BC=1) creates strong feedback to rates of methanogenesis and iron reduction. Reference simulations were based on soils with 30% SOC (water content=2 g g⁻¹ dwt, and pH=5).

Deleted: 10

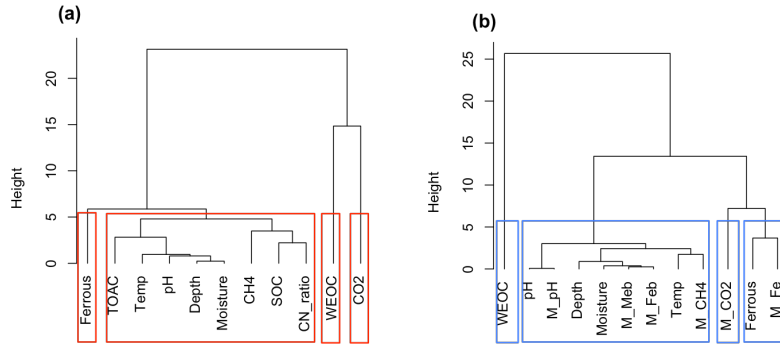
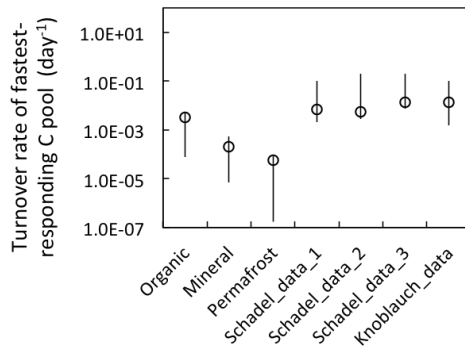


Figure 8. Cluster analysis of soil geochemical properties related to CO_2 and CH_4 production using Ward's linkage method.

Deleted: 11

(a) cluster analysis of measured soil geochemical characteristics and observed CO_2 and CH_4 production ($n=42$); (b) cluster analysis of modeled results ($n=42$). Model simulated CO_2 , CH_4 , and Fe(II) production and final pH are labeled as M_CO_2 , M_CH_4 , M_Fe , and M_pH , respectively. Biomass of methanogens and iron reducers were tracked in the model and labeled as M_Meb and M_Feb , respectively.



5 **Figure 2.** Model estimated turnover rates of the fastest-decomposing carbon pool. Organic, Mineral, and Permafrost labels
 represent estimations from our model simulations ([rates](#), estimated at 4 °C). Schadel_data represent turnover rates
 estimated via a three-pool model from pooled anaerobic incubations with normalized incubation temperature of 5 °C (tag
 1, 2, and 3 represent pool estimation from different soil types: 1. Organic, 2. Mineral <1m, 3. Mineral >1m) .
 Knoblauch_data are rate estimates (at 4 °C) made via a two-pool model (Schädel et al., 2014;Knoblauch et al., 2013). Open
 10 symbols represent the average values, and the vertical lines represent the estimated range.

Deleted: 12

Deleted: Rate

Deleted: 

Page 10: [1] Deleted	Revised	6/8/18 5:25:00 PM
-----------------------------	----------------	--------------------------

The fate of permafrost C is determined in large part by soil moisture, particularly water saturation caused by ice melting, precipitation, infiltration and runoff (Riley et al., 2011; Elberling et al., 2013; Schädel et al., 2016). Permafrost thaw frequently creates large areas of soil inundation due to abrupt surface collapse and subsidence (Painter et al., 2013; Walvoord and Kurylyk, 2016), resulting in higher levels of CH₄ production via anaerobic decomposition pathways. Although total carbon release under oxic conditions is much higher than under anoxic conditions (Schädel et al., 2016), emissions of high global warming potential CH₄ may offset reduced lower CO₂ emissions in the absence of oxygen (Lee et al., 2012).

Page 16: [2] Deleted	Revised	6/8/18 5:25:00 PM
-----------------------------	----------------	--------------------------

3a). Higher incubation temperatures showed minimal effect on the WEOC/SOC quotient, and a temperature response trend remained insignificant.

Page 16: [3] Deleted	Revised	6/8/18 5:25:00 PM
-----------------------------	----------------	--------------------------

from LCP and HCP centers (Figure 3b). In most mineral soils

Page 16: [4] Deleted	Revised	6/8/18 5:25:00 PM
-----------------------------	----------------	--------------------------

%, partially contributing to the depletion of WEOC after the anoxic incubations.

Page 16: [5] Deleted	Revised	6/8/18 5:25:00 PM
-----------------------------	----------------	--------------------------

Good correlations between soil organic carbon (SOC, WEOC and TOAC) and soil moisture were found, indicating the importance of soil moisture in controlling carbon substrate availability (Table 1). High organic carbon content and high soil moisture are associated with organic and permafrost soil, while mineral soils are much drier with lower organic carbon content (Figure S2). Fe(II) concentration is measured as a proxy of soil redox potential, and it is most closely related to soil pH (Table 1).

3.2

Page 16: [6] Deleted	Revised	6/8/18 5:25:00 PM
-----------------------------	----------------	--------------------------

response and soil layer effects

Cumulative production of both CO₂ and CH₄ showed close correlation with soil carbon content (represented as SOC, WEOC and TOAC) on a dry soil mass basis, as well as soil moisture (Table S4). Given the high inter-correlation among these soil attributes (Table 1), we evaluated the relationship between gas production and soil geochemical characteristics on per gram C basis to avoid inter-correlation caused by SOC content (Lee et al., 2012). The maximum values of cumulative CO₂ production were 756 and 534 µmol g⁻¹ C at 8 and -2°C, exceeding the median values at corresponding temperature by 5 and 8 times, respectively. The maximum cumulative CH₄ production was 198 µmol g⁻¹ C from the organic layer of LCP center at 8 °C, approximately 123 times the median value among the rest of the samples. Cumulative CH₄ production from the same soil was 9.2 µmol g⁻¹ C when incubated at -2 °C, 9 times the median rate among the remaining samples. Cumulative CO₂ production showed strong positive correlation with initial soil moisture at both 8 and -2 °C, while cumulative CH₄ production only correlated with initial soil moisture at 8 °C

(Table 1). Noticeably, significant correlation between production of CO₂ and CH₄ was found at 8 °C, but not at -2 °C (Table 1), suggesting CO₂ and CH₄ production were controlled by different factors at 8 and -2 °C, respectively. Given that cumulative CO₂ and CH₄ production both had skewed distributions among samples (Figure S3), the significance in the correlation between gas production and moisture would be substantially weaker with exclusion of measurements from the wet organic layer of LCP center.

Initial production rates of CO₂ and CH₄ varied significantly across organic, mineral and permafrost soil layers

Page 16: [7] Deleted	Revised	6/8/18 5:25:00 PM
<0.001 and p<0.001, respectively, Figure 4). Temperature showed a substantial positive effect on CO ₂ and CH ₄ production rates (p		

Page 16: [8] Deleted	Revised	6/8/18 5:25:00 PM
). A significant temperature × soil layer interaction effect was found on CO ₂ production rate, but not on CH ₄ production rate (Table S5), suggesting CH ₄ production might be more sensitive to constraints from additional environmental conditions.		

A

Page 16: [9] Formatted	Revised	6/8/18 5:25:00 PM
Font: Font color: Dark Gray, Border: : (No border), Pattern: Clear (White)		

Page 16: [10] Deleted	Revised	6/8/18 5:25:00 PM
value was calculated for each condition to further assess the temperature dependency of CO ₂ and CH ₄ production (Figure S4). The calculated Q ₁₀ values of CO ₂ production from organic soil were within a		

Page 16: [11] Deleted	Revised	6/8/18 5:25:00 PM
between 4.6 and 5.0. Mineral soils with lower SOC content showed a wider range of Q ₁₀ values (from 3.6 to 7.3). Permafrost showed significantly lower Q ₁₀ than both organic and mineral layers (Table S6). Methanogenesis		

Page 16: [12] Deleted	Revised	6/8/18 5:25:00 PM
, while in mineral soils and permafrost, the average Q ₁₀ values were 7.1 and 1.6, respectively.		

Page 16: [13] Formatted	Revised	6/8/18 5:25:00 PM
Font: Font color: Black, Border: : (No border), Pattern: Clear		

Page 16: [14] Deleted	Revised	6/8/18 5:25:00 PM
-----------------------	---------	-------------------

Page 16: [15] Formatted	Revised	6/8/18 5:25:00 PM
Space Before: 24 pt, Line spacing: 1.5 lines		

Page 23: [16] Deleted	Revised	6/8/18 5:25:00 PM
+		

Page 23: [16] Deleted	Revised	6/8/18 5:25:00 PM
	+	
Page 23: [16] Deleted	Revised	6/8/18 5:25:00 PM
	+	
Page 23: [16] Deleted	Revised	6/8/18 5:25:00 PM
	+	
Page 23: [17] Deleted	Revised	6/8/18 5:25:00 PM
	+	
Page 23: [17] Deleted	Revised	6/8/18 5:25:00 PM
	+	
Page 23: [17] Deleted	Revised	6/8/18 5:25:00 PM
	+	
Page 23: [17] Deleted	Revised	6/8/18 5:25:00 PM
	+	
Page 23: [18] Deleted	Revised	6/8/18 5:25:00 PM
	HC	
Page 23: [18] Deleted	Revised	6/8/18 5:25:00 PM
	HC	
Page 23: [18] Deleted	Revised	6/8/18 5:25:00 PM
	HC	
Page 23: [18] Deleted	Revised	6/8/18 5:25:00 PM
	HC	
Page 23: [19] Deleted	Revised	6/8/18 5:25:00 PM
	+	
Page 23: [19] Deleted	Revised	6/8/18 5:25:00 PM
	+	
Page 23: [19] Deleted	Revised	6/8/18 5:25:00 PM
	+	
Page 23: [19] Deleted	Revised	6/8/18 5:25:00 PM
	+	
Page 23: [20] Deleted	Revised	6/8/18 5:25:00 PM
	+	
Page 23: [20] Deleted	Revised	6/8/18 5:25:00 PM
	+	
Page 23: [21] Deleted	Revised	6/8/18 5:25:00 PM

We used the CLM_CN temperature response function (B1) in our simulations (Thornton and Rosenbloom, 2005). Additional temperature response functions tested here including B2 used by CENTURY model (Parton et al., 2001), Arrhenius equation B3 used in ecosys (Grant, 1998), and the quadratic equation B4 (Ratkowsky et al., 1983). T_{ref} is set at 25 °C, E_a is the activation energy (J mol⁻¹), R is the universal gas constant (J K⁻¹ mol⁻¹). T_m used in Ratkowsky model represents the conceptual temperature of no metabolic significant, and is set at -8 °C in this study.

Page 23: [22] Formatted	Revised	6/8/18 5:25:00 PM
-------------------------	---------	-------------------

Left, Tab stops: 3.5", Centered + 6.5", Left

Page 23: [23] Formatted	Revised	6/8/18 5:25:00 PM
-------------------------	---------	-------------------

Left, Tab stops: 3.31", Centered + 3.75", Centered + 6.5", Left + Not at 3" + 5.69"

Page 23: [24] Formatted	Revised	6/8/18 5:25:00 PM
-------------------------	---------	-------------------

Left, Tab stops: 3.5", Centered + 6.5", Left

Page 23: [25] Deleted	Revised	6/8/18 5:25:00 PM
-----------------------	---------	-------------------

=

Page 23: [25] Deleted	Revised	6/8/18 5:25:00 PM
-----------------------	---------	-------------------

=

Page 23: [26] Formatted	Revised	6/8/18 5:25:00 PM
-------------------------	---------	-------------------

Left, Tab stops: 3.5", Centered + 6.5", Left + Not at 0.39" + 0.78" + 1.17" + 1.56" + 1.94" + 2.33" + 2.72" + 3.11" + 3.89" + 4.28" + 4.67"

Page 23: [27] Deleted	Revised	6/8/18 5:25:00 PM
-----------------------	---------	-------------------

Page 23: [27] Deleted	Revised	6/8/18 5:25:00 PM
-----------------------	---------	-------------------

Page 23: [28] Formatted	Revised	6/8/18 5:25:00 PM
-------------------------	---------	-------------------

Indent: First line: 0.5", Tab stops: 3.5", Centered

Page 27: [29] Deleted	Revised	6/8/18 5:25:00 PM
-----------------------	---------	-------------------

Table 1. Descriptive statistics and correlation matrix for soil geochemical characteristics, labile carbon pool (in $\mu\text{mol g}^{-1}$ C) and estimated 60 days max production of CO_2 and CH_4 (in $\mu\text{mol g}^{-1}$ C) at 8 and -2°C.

	1	2	3	4	5	6	7	8a/8b
1. SOC								
2. WEOC	0.80 ^a							
3. TOAC	0.62 ^b	0.69 ^a						
4. Moisture	0.69 ^a	0.82 ^a	0.78 ^a					
5. pH	-0.30	-0.15	-0.14	-0.11				
6. C/N ratio	0.07	0.06	0.17	0.05	-0.64 ^b			
7. Fe(II)	0.06	0.09	0.15	0.04	-0.35	-0.03		
8a. Max_8_CO ₂	0.38	0.39	0.33	0.63 ^b	-0.09	-0.13	-0.33	
8b. Max_2_CO ₂	0.40	0.54 ^b	0.67 ^a	0.79 ^a	0.07	-0.14	-0.30	
9a. Max_8_CH ₄	0.31	0.41	0.50	0.74 ^a	-0.24	0.18	-0.29	0.88 ^a
9b. Max_2_CH ₄	-0.33	-0.24	-0.08	0.06	0.19	-0.31	-0.32	0.35

Note: ^a correlation is significant at the 0.01 level (two-tailed); ^b correlation is significant at the 0.05 level (two-tailed)

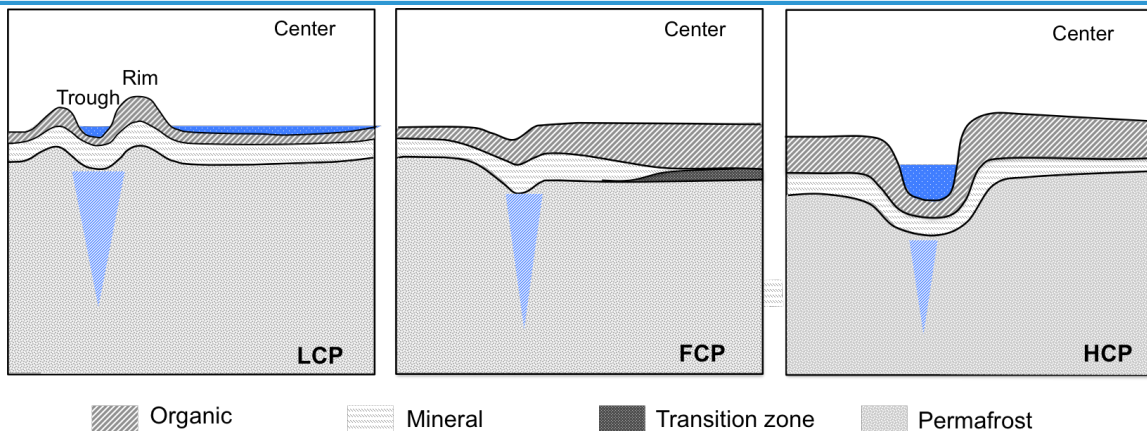


Figure 1. Schematic diagrams of different polygon types and features. The cross section represents the relative landscape positions of soil profile, including organic, mineral, transition zone and permafrost.

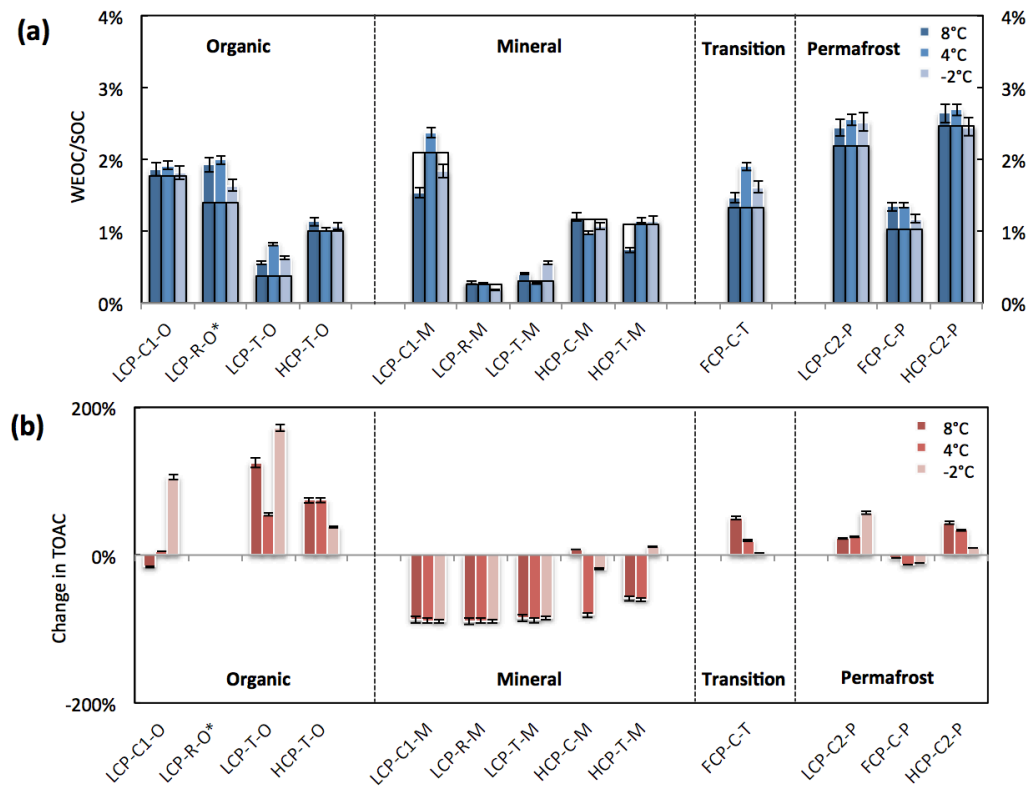


Figure 3. Changes in (a) WEOC/SOC (quotient of water extractable organic carbon to total soil organic carbon) and (b) TOAC (calculated as $(TOAC_{after} - TOAC_{before})/TOAC_{before}$) after anaerobic incubations at -2, 4 and 8 °C. Bars framed with black lines in panel (a) represent the TOAC/WEOC levels before incubation, and blue bars represent levels after the incubation at corresponding temperatures. Error bars represent standard deviations among triplicate measurements.